AIAA JOURNAL
Vol. 46, No. 6, June 2008

Vibroacoustic Modes and Active Control of Both Vibration and Sound

Tsutomu Kaizuka* and Nobuo Tanaka†
Tokyo Metropolitan University, Tokyo 191-0065, Japan

DOI: 10.2514/1.32706

Vibration reduction and sound reduction are not necessarily compatible. The sum of the structural kinetic energy and acoustic power in free space (acoustic potential energy in an enclosed space) is an error criterion to control both vibration and sound. The orthogonal contributors with respect to the sum, "vibroacoustic modes" and the frequency dependent spatial filters, which can estimate the amplitudes of the vibroacoustic modes, "vibroacoustic modal filters," are formulated. Vibroacoustic modal filters allow a controller to coordinate both vibration and sound reduction and achieve order reduction. However, the implementation is not very easy because of the frequency dependence. The frequency independent vibroacoustic modal filters are formulated by omitting the frequency dependence. The omission of the frequency dependence mathematically proves to be valid for baffled structures in free space. Moreover, the developed theories are applied to baffled rectangular plates in free space, and the simulation results, for example, the contributions of the vibroacoustic modes to the sum of the structural kinetic energy and acoustic power, the shapes of the vibroacoustic modes, and the performance of the feedforward control using the frequency independent vibroacoustic modal filters, are presented.

Nomenclature

c_0	=	speed of sound in the air
$\mathbf{E}_e$	=	unity matrix in elemental radiator form
$\mathbf{E}_s$	=	unity matrix in structural mode form
$J_{\text{acoustic}}(\omega)$	=	time-averaged acoustic power (acoustic potential energy) after control
$J'_{\text{acoustic}}(\omega)$	=	time-averaged acoustic power (acoustic potential energy) before control
$J_{\text{vibro}}(\omega)$	=	time-averaged structural kinetic energy after control
$J'_{\text{vibro}}(\omega)$	=	time-averaged structural kinetic energy before control
$J_{\text{vibroacoustic}}(\omega)$	=	error criterion
k	=	acoustic wave number
L	=	number of the elemental radiators
M	=	number of the structural modes
$\mathbf{M}$	=	diagonal matrix whose terms are the square roots of the halves of the masses of the elemental radiators
$\mathbf{Q}_e(\omega)$	=	matrix whose columns are the shapes of the vibroacoustic modes, that is, the modal filters, in elemental radiator form
$\mathbf{Q}_s(\omega)$	=	matrix whose columns are the shapes of the vibroacoustic modes, that is, the modal filters, in structural mode form
$\mathbf{R}(\omega)$	=	matrix whose terms are the acoustic transfer functions between the elemental radiators
$\mathbf{R}_e(\omega)$	=	matrix whose terms are the products of the acoustic transfer functions between the elemental radiators and the square roots of the halves of the masses of the elemental radiators
$\mathbf{R}_e(\omega)$	=	matrix whose terms are the acoustic transfer functions between the structural modes
$\mathbf{r}_l$	=	representative location of the lth elemental radiator
$\mathbf{v}(\omega)$	=	vector whose terms are the normal velocities of the elemental radiators
$\mathbf{v}_e(\omega)$	=	vector whose terms are the products of the normal velocities and the square roots of the halves of the masses of the elemental radiators
$\mathbf{v}_s(\omega)$	=	vector whose terms are the normal velocities of the structural modes
$\mathbf{w}_e(\omega)$	=	vector whose terms are the amplitudes of the vibroacoustic modes in elemental radiator form
$\mathbf{w}'_e(\omega)$	=	vector whose terms are the amplitudes of the vibroacoustic modes, which are estimated by the frequency independent modal filters, in elemental radiator form
$\mathbf{w}_s(\omega)$	=	vector whose terms are the amplitudes of the vibroacoustic modes in structural mode form
$\mathbf{w}'_s(\omega)$	=	vector whose terms are the amplitudes of the vibroacoustic modes, which are estimated by the frequency independent modal filters, in structural mode form
$\mathbf{w}''_s(\omega)$	=	vector whose terms are the amplitudes of the vibroacoustic modes, which are estimated by the vibroacoustic modal filters and PVDF smart sensors as the structural modal filters, in structural mode form
$\mathbf{w}'''_s(\omega)$	=	vector whose terms are the amplitudes of the vibroacoustic modes, which are estimated by PVDF smart sensors as the frequency independent vibroacoustic modal filters, in structural mode form
$\alpha(\omega)$	=	weighting factor
$\alpha_e(w)$	=	weighting factor in elemental radiator form
$\alpha_s(\omega)$	=	weighting factor in structural mode form
ΔS	=	area of the elemental radiator
$\mathbf{\Lambda}_e(\omega)$	=	diagonal matrix whose terms are the contributions of the vibroacoustic modes to the error criterion, that is, the weighting filters, in elemental radiator form
$\mathbf{\Lambda}_s(\omega)$	=	diagonal matrix whose terms are the contributions of the vibroacoustic modes to the error criterion, that is, the weighting filters, in structural mode form

Received 9 June 2007; revision received 11 November 2007; accepted for publication 14 November 2007.

*Ph.D. Candidate, Division of Aerospace Engineering, 6-6 Hino, also Research Fellow DC1, Japan Society for the Promotion of Science.

†Professor, Division of Aerospace Engineering, 6-6 Hino.

ρ_0 = density of air
$\mathbf{\Psi}$ = matrix whose terms are dependent on the shapes of the structural modes and the locations of the elemental radiators
$\mathbf{\Omega}_e(\omega)$ = diagonal matrix whose terms are the contributions of the vibroacoustic modes to the acoustic power (acoustic potential energy) in elemental radiator form
$\mathbf{\Omega}_s(\omega)$ = diagonal matrix whose terms are the contributions of the vibroacoustic modes to the acoustic power (acoustic potential energy) in structural mode form
ω = angular frequency

I. Introduction

VIBROACOUSTIC control is an important issue in aerospace vehicles [1–11]. Vibrations damage the aircraft fuselage and rocket fairing, and sound jeopardizes aircraft cabin comfort and rocket payload safety. However, vibration and sound reduction are not necessarily compatible [12–18]. Vibration reduction can cause an increase in sound, and sound reduction can cause an increase in vibration. For example, active structural acoustic control, which consists of structural actuators and acoustic sensors, could increase the vibration of the aircraft fuselage while reducing the sound in the cabin [8]. The increased vibration could produce cracks in the fuselage, then enlarge the cracks, and, finally, bring the aircraft to failure. For controlling both vibration and sound, the error criterion should be the sum of the structural kinetic energy and acoustic power in free space (acoustic potential energy in an enclosed space).

It is meaningful to formulate the orthogonal contributors with respect to the error criterion of interest. In the case in which the error criterion is the structural kinetic energy, any knowledge about the structural modes, which are the orthogonal contributors with respect to the structural kinetic energy, is useful for controller design [19–25]. Similarly, in the case in which the error criterion is the acoustic power (acoustic potential energy), any knowledge about the radiation modes, which are the orthogonal contributors with respect to the acoustic power (acoustic potential energy), is useful when designing controllers [26–38]. However, in the case in which the error criterion is the sum of the structural kinetic energy and acoustic power (acoustic potential energy), the orthogonal contributors are unclear.

The primary objective of this paper is to formulate the orthogonal contributors with respect to the sum of the structural kinetic energy and acoustic power (acoustic potential energy), termed "vibroacoustic modes," in two forms: elemental radiator and structural mode. In the elemental radiator form, the surface of the vibrating structure is assumed to consist of a number of elemental radiators, and the vibroacoustic modes are formulated in terms of the elemental radiators. In the structural mode form, the behavior of the vibrating structure is assumed to consist of a number of structural modes, and the vibroacoustic modes are formulated in terms of the structural modes.

The second objective of this paper is to formulate spatial filters to estimate the amplitudes of the vibroacoustic modes, termed "vibroacoustic modal filters," in both elemental radiator and structural mode forms. In the elemental radiator form, the vibroacoustic modal filters are derived from the masses of the elemental radiators and the acoustic transfer functions between these radiators. Subsequently, the amplitudes of the vibroacoustic modes are estimated by passing the measured normal velocities of the elemental radiators to the vibroacoustic modal filters. In the structural mode form, the vibroacoustic modal filters are derived from the shapes of the structural modes and the acoustic transfer functions between the structural modes. The amplitudes of the vibroacoustic modes are then estimated by passing the measured normal velocities of the structural modes to the vibroacoustic modal filters. In both forms, the vibroacoustic modal filters are frequency dependent, as is clear from the fact that these filters are related to the acoustic transfer functions. Therefore, the vibroacoustic modal filters consist of higher order digital filters, and their implementations are not very easy.

The third objective of this paper is to formulate frequency independent vibroacoustic modal filters in elemental radiator and structural mode forms, omitting the frequency dependence. As mentioned previously, the frequency dependence of the vibroacoustic modal filters is related to the acoustic transfer function. Hence, the omission of the frequency dependence should be validated for the respective acoustic fields, for example, baffled structures in free space, three-dimensional structures in free space, and three-dimensional structures in an enclosed space. Baffled structures in free space are addressed in this paper to simplify the acoustic transfer functions from an academic point of view. However, three-dimensional structures in an enclosed space are faithful to real aerospace vehicles, that is, the insides of the aircraft fuselage and rocket fairing, and thus these structures should be addressed in future works from a practical point of view. The work presented here is the first step in demonstrating the feasibility of frequency independent vibroacoustic modal filters.

In Sec. II, the vibroacoustic modes and vibroacoustic modal filters are formulated. In Sec. III, the frequency independent vibroacoustic modal filters are formulated for baffled structures in free space. In Sec. IV, the developed theories are applied to baffled rectangular plates in free space, and the simulation results, for example, the contributions of the vibroacoustic modes to the sum of the structural kinetic energy and acoustic power, the shapes of the vibroacoustic modes, and the performance of the optimal feedforward control using the frequency independent vibroacoustic modal filters, are presented and discussed. In Sec. V, the significance of this paper is summarized.

The mathematical process for deriving the vibroacoustic modes and vibroacoustic modal filters is based on diagonalization, and the approach is expanded from one used for deriving the radiation modes and radiation modal filters. The referential literatures [26–38] are relevant.

II. Vibroacoustic Modes and Vibroacoustic Modal Filters

First, the error criterion for controlling both vibration and sound $J_{\text{vibroacoustic}}(\omega)$ is defined as follows:

$$J_{\text{vibroacoustic}}(\omega) = \alpha(\omega) J_{\text{vibro}}(\omega) + J_{\text{acoustic}}(\omega) \tag{1}$$

where $J_{\text{vibro}}(\omega)$ is the time-averaged structural kinetic energy after control; $J_{\text{acoustic}}(\omega)$ is the time-averaged acoustic power in free space (acoustic potential energy in an enclosed space) after control; $\alpha(\omega)$ is the positive real weighting factor between the structural kinetic energy and acoustic power (acoustic potential energy), which is a dimensional quantity with a unit of inverse second in free space (nondimensional quantity in an enclosed space); and ω is the angular frequency. The different order of magnitudes of the structural kinetic energy and acoustic power (acoustic potential energy) is a serious problem. For instance, if the magnitude of the structural kinetic energy is much larger than that of the acoustic power (acoustic potential energy), the sum is nearly equal to the structural kinetic energy and therefore is not effective as the error criterion for controlling sound as well as vibration. The weighting factor plays a role in balancing the different orders of magnitude. The weighting factor, which can be set a priori, will be presented hereinafter. This weighting factor is dependent only on the inherent properties of the system of interest and is independent of the properties of the disturbance, for example, the distribution and frequency characteristics, and it may be advantageous in aerospace vehicles surrounded by a changing environment.

It should be noted that there exists a possible alternative definition of the error criterion:

$$J_{\text{vibroacoustic}}(\omega) = \frac{J_{\text{vibro}}(\omega)}{J'_{\text{vibro}}(\omega)} + \frac{J_{\text{acoustic}}(\omega)}{J'_{\text{acoustic}}(\omega)} \tag{2}$$

where $J'_{\text{vibro}}(\omega)$ is the time-averaged structural kinetic energy before control, and $J'_{\text{acoustic}}(\omega)$ is the time-averaged acoustic power (acoustic potential energy) before control. The first term in Eq. (2) is the

reduction ratio of the structural kinetic energy before and after control, and the second term is the reduction ratio of the acoustic power (acoustic potential energy) before and after control. This formulation provides a palpable yardstick of what percent reduction of vibration and sound is actually gained, and it is an advantage of having the properties of the disturbance in view. On the other hand, Eq. (1) hides the yardstick, and it is a disadvantage of leaving the properties of the disturbance out of view. The different orders of magnitude of the structural kinetic energy and acoustic power (acoustic potential energy) are balanced by summing not the magnitudes but the reduction ratios. Because the reduction ratios vary with the properties of the disturbance, this weighting cannot be set a priori. In other words, this weighting must be reset when the properties of the disturbance are changed, and it may be disadvantageous in aerospace vehicles surrounded by a changing environment.

Although Eqs. (1) and (2), respectively, have the advantage and disadvantage, Eq. (1) is employed in this paper from the standpoint of attaching importance to the a priori feature.

The vibroacoustic modes and vibroacoustic modal filters are formulated as follows: Sec. II.A, elemental radiator form; and Sec. II.B, structural mode form.

A. Elemental Radiator Form

It is assumed that the surface of the vibrating structure is divided into L elemental radiators, and the acoustic reciprocity holds. Equation (1) is then expanded as [29]

$$J_{\text{vibroacoustic}}(\omega) = \mathbf{v}^H(\omega)\{\alpha_e(\omega)\mathbf{M}\mathbf{M} + \mathbf{R}(\omega)\}\mathbf{v}(\omega) \tag{3}$$

where $\mathbf{v}(\omega)$ is the $(L \cdot 1)$ and complex vector, whose terms are the normal velocities at the representative locations of the elemental radiators; $\mathbf{M}$ is the $(L \cdot L)$, real, diagonal, and positive definite matrix, whose terms are the square roots of halves of the masses of the elemental radiators; $\mathbf{R}(\omega)$ is the $(L \cdot L)$, real, symmetric, and positive definite matrix, whose terms are the acoustic transfer functions between the representative locations of the elemental radiators; $\alpha_e(\omega)$ is the positive real weighting factor; and superscript H is the conjugate transpose. Equation (3) is rewritten as

$$J_{\text{vibroacoustic}}(\omega) = \mathbf{v}_e^H(\omega)\{\alpha_e(\omega)\mathbf{E}_e + \mathbf{R}_e(\omega)\}\mathbf{v}_e(\omega) \tag{4}$$

where $\mathbf{v}_e(\omega)$ is the $(L \cdot 1)$ and complex vector defined as

$$\mathbf{v}_e(\omega) = \mathbf{M}\mathbf{v}(\omega) \tag{5}$$

$\mathbf{E}_e$ is the $(L \cdot L)$ unit matrix, and $\mathbf{R}_e(\omega)$ is the $(L \cdot L)$, real, symmetric, and positive definite matrix defined as

$$\mathbf{R}_e(\omega) = \mathbf{M}^{-1}\mathbf{R}(\omega)\mathbf{M}^{-1} \tag{6}$$

Because $\{\alpha_e(\omega)\mathbf{E}_e + \mathbf{R}_e(\omega)\}$ in Eq. (4) is real, symmetric, and positive definite, it can be diagonalized as

$$\begin{aligned}\mathbf{Q}_e^T(\omega)\{\alpha_e(\omega)\mathbf{E}_e + \mathbf{R}_e(\omega)\}\mathbf{Q}_e(\omega) \\ = \alpha_e(\omega)\mathbf{E}_e + \mathbf{Q}_e^T(\omega)\mathbf{R}_e(\omega)\mathbf{Q}_e(\omega) \\ = \alpha_e(\omega)\mathbf{E}_e + \mathbf{\Omega}_e(\omega) = \mathbf{\Lambda}_e(\omega)\end{aligned} \tag{7}$$

where $\mathbf{\Omega}_e(\omega)$ is the $(L \cdot L)$, real, diagonal, and positive definite matrix, whose terms are the eigenvalues of $\mathbf{R}_e(\omega)$; $\mathbf{\Lambda}_e(\omega)$ is the $(L \cdot L)$, real, diagonal, and positive definite matrix, whose terms are the eigenvalues of $\{\alpha_e(\omega)\mathbf{E}_e + \mathbf{R}_e(\omega)\}$; $\mathbf{Q}_e(\omega)$ is the $(L \cdot L)$, real, and orthogonal matrix, whose columns are the eigenvectors of $\mathbf{R}_e(\omega)$ as well as $\{\alpha_e(\omega)\mathbf{E}_e + \mathbf{R}_e(\omega)\}$; and superscript T is the transpose. Substituting Eq. (7) into Eq. (4) yields

$$J_{\text{vibroacoustic}}(\omega) = \mathbf{w}_e^H(\omega)\mathbf{\Lambda}_e(\omega)\mathbf{w}_e(\omega) \tag{8}$$

where $\mathbf{w}_e(\omega)$ is an $(L \cdot 1)$ and complex vector defined as

$$\mathbf{w}_e(\omega) = \mathbf{Q}_e^T(\omega)\mathbf{v}_e(\omega) \tag{9}$$

Equations (8) and (9) indicate the orthogonal contributors with respect to the error criterion, that is, the vibroacoustic modes: the terms of $\mathbf{\Lambda}_e(\omega)$ are the contributions of the vibroacoustic modes to the error criterion; the columns of $\mathbf{Q}_e(\omega)$ are the shapes of the vibroacoustic modes; and the terms of $\mathbf{w}_e(\omega)$ are the amplitudes of the vibroacoustic modes. The indexes of the vibroacoustic modes are defined in descending order in relation to the contributions. The error criterion can then be approximated by the sum of the lower order vibroacoustic modes, and this approximation, that is, order reduction, is desirable in practice.

Equations (8) and (9) also indicate the procedure used to obtain the error criterion, as illustrated in Fig. 1a. First, the terms of $\mathbf{v}_e(\omega)$, that is, the gained normal velocities of the elemental radiators, are measured by a number of discrete sensors. Then, the terms of $\mathbf{w}_e(\omega)$, that is, the amplitudes of the vibroacoustic modes, are estimated by passing the measured velocities to the columns of $\mathbf{Q}_e(\omega)$, that is, the vibroacoustic modal filters. Finally, the error criterion is calculated by passing the estimated amplitudes to the terms of $\mathbf{\Lambda}_e(\omega)$, that is, the weighting filters, and summing the products. The advantage of using the elemental radiator form is that no knowledge about the structural modes is required. The disadvantage of this form is that a number of discrete sensors are required, and the computation labor for the vibroacoustic modal filters is unavoidable. In addition, the vibroacoustic modal and weighting filters consist of digital filters, rather than fixed gains, due to their frequency dependence. The vibroacoustic modal filters consisting of higher order digital filters are not very practical, whereas the weighting filters consisting of lower order digital filters are practical. Therefore, the vibroacoustic modal filters should consist of fixed gains, omitting the frequency dependence. In Sec. III.A, frequency independent vibroacoustic modal filters are formulated for baffled structures in free space.

Moreover, Eq. (7) indicates that the terms of $\alpha_e(\omega)\mathbf{E}_e$ are the contributions of the vibroacoustic modes to the structural kinetic energy, and the terms of $\mathbf{\Omega}_e(\omega)$ are the contributions of the vibroacoustic modes to the acoustic power (acoustic potential energy). The contributions to the structural kinetic energy are uniform in the vibroacoustic modes, whereas the contributions to the acoustic power (acoustic potential energy) are varied in these modes. The magnitude of the contributions to the structural kinetic energy and that of the contributions to the acoustic power (acoustic potential energy) may be of a different order, mainly because the magnitudes of the structural kinetic energy and the acoustic power (acoustic potential energy) are usually different. The terms of $\mathbf{\Lambda}_e(\omega)$, that is, the weighting filters, have been defined as the sum of the contributions to the structural kinetic energy and those to the acoustic power (acoustic potential energy) for the purpose of controlling both vibration and sound. Here, the different orders of magnitude of the contributions pose a problem. For instance, if the magnitude of the contributions to the structural kinetic energy is much larger than that of the contributions to the acoustic power (acoustic potential energy), the sum is nearly equal to the contributions to the structural kinetic energy and neither makes sense nor provides the answers for the intended purpose. The weighting factor plays a role in balancing the different orders of magnitudes. A proper weighting factor is set as

$$\alpha_e(\omega) = \frac{\text{trace}\{\mathbf{\Omega}_e(\omega)\}}{L} = \frac{\text{trace}\{\mathbf{R}_e(\omega)\}}{L} \tag{10}$$

The terms of $\mathbf{R}(\omega)$ are the dimensional quantities with units of kg/s in free space (kg in an enclosed space), as is clear from Eq. (3), and the terms of $\mathbf{R}_e(\omega)$ are the dimensional quantities with units of $1/s$ in free space (nondimensional quantities in an enclosed space), as is clear from Eq. (6). Hence, the weighting factor is a dimensional quantity with the unit of $1/s$ in free space (nondimensional quantity in an enclosed space). Equation (10) indicates that the magnitude of the contributions to the structural kinetic energy is adjusted as the basis for estimating the average of the contributions to the acoustic power (acoustic potential energy). The weighting factor does not change with the disturbance properties, thus this setting method is a priori. The weighting factor does not affect the vibroacoustic modal filters, but it affects the weighting filters, as is clear from Eq. (7).

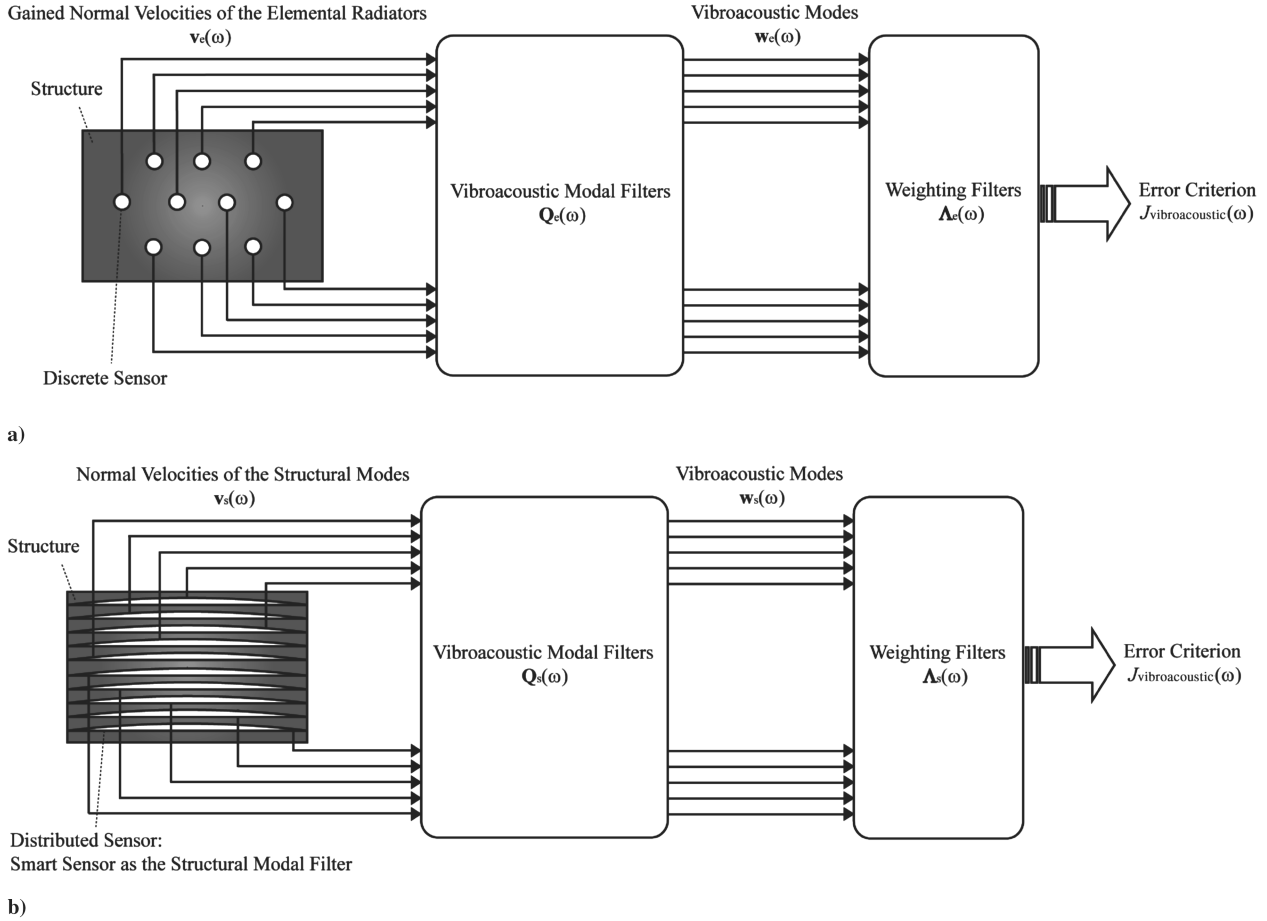

Fig. 1 Measurement systems using the vibroacoustic modal filters and weighting filters: a) elemental radiator form, and b) structural mode form.

Equations (6–9) indicate that if the terms of $\mathbf{M}$ are uniform, which means that the masses of the elemental radiators are uniform, the terms of $\mathbf{\Omega}_e(\omega)$ are proportional to the radiation efficiencies of the radiation modes, the columns of $\mathbf{Q}_e(\omega)$ are the shapes of the radiation modes, and the terms of $\mathbf{w}_e(\omega)$ are the amplitudes of the radiation modes [29]. In this case, the contributions of the vibroacoustic modes to the error criterion are the sum of the weighting factor and the values proportional to the radiation efficiencies of the radiation modes, and the shapes and amplitudes of the vibroacoustic modes are the same as those of the radiation modes.

B. Structural Mode Form

It is assumed that the behavior of the vibrating structure is described by M structural modes. The normal velocities of the elemental radiators are then written as

$$\mathbf{v}(\omega) = \mathbf{\Psi}^T \mathbf{v}_s(\omega) \tag{11}$$

where $\mathbf{\Psi}$ is the $(M \cdot L)$ real matrix, whose terms are dependent on the shapes of the structural modes and the representative locations of the elemental radiators; and $\mathbf{v}_s(\omega)$ is the $(M \cdot 1)$ complex vector, whose terms are the normal velocities of the structural modes. Furthermore, it is assumed that the shapes of the structural modes are normalized with respect to the halves of the modal masses. Substituting Eq. (11) into Eq. (3) yields

$$J_{\text{vibroacoustic}}(\omega) = \mathbf{v}_s^H(\omega)\{\alpha_s(\omega)\mathbf{E}_s + \mathbf{R}_s(\omega)\}\mathbf{v}_s(\omega) \tag{12}$$

where $\mathbf{E}_s$ is the $(M \cdot M)$ unit matrix, $\mathbf{R}_s(\omega)$ is the $(M \cdot M)$, real, symmetric, and positive definite matrix defined as

$$\mathbf{R}_s(\omega) = \mathbf{\Psi}\mathbf{R}(\omega)\mathbf{\Psi}^T \tag{13}$$

Here, $\alpha_s(\omega)$ is a positive real weighting factor, and the orthogonality of the structural modes is used for the derivation of Eq. (12). Because $\{\alpha_s(\omega)\mathbf{E}_s + \mathbf{R}_s(\omega)\}$ in Eq. (12) is real, symmetric, and positive definite, it can be diagonalized as

$$\mathbf{Q}_s^T(\omega)\{\alpha_s(\omega)\mathbf{E}_s + \mathbf{R}_s(\omega)\}\mathbf{Q}_s(\omega) = \alpha_s(\omega)\mathbf{E}_s + \mathbf{Q}_s^T(\omega)\mathbf{R}_s(\omega)\mathbf{Q}_s(\omega) = \alpha_s(\omega)\mathbf{E}_s + \mathbf{\Omega}_s(\omega) = \mathbf{\Lambda}_s(\omega) \tag{14}$$

where $\mathbf{\Omega}_s(\omega)$ is the $(M \cdot M)$, real, diagonal, and positive definite matrix, whose terms are the eigenvalues of $\mathbf{R}_s(\omega)$; $\mathbf{\Lambda}_s(\omega)$ is the $(M \cdot M)$, real, diagonal, and positive definite matrix, whose terms are the eigenvalues of $\{\alpha_s(\omega)\mathbf{E}_s + \mathbf{R}_s(\omega)\}$; and $\mathbf{Q}_s(\omega)$ is the $(M \cdot M)$, real, and orthogonal matrix, whose columns are the eigenvectors of $\mathbf{R}_s(\omega)$ as well as $\{\alpha_s(\omega)\mathbf{E}_s + \mathbf{R}_s(\omega)\}$. Substituting Eq. (14) into Eq. (12)

$$J_{\text{vibroacoustic}}(\omega) = \mathbf{w}_s^H(\omega)\mathbf{\Lambda}_s(\omega)\mathbf{w}_s(\omega) \tag{15}$$

where $\mathbf{w}_s(\omega)$ is a $(M \cdot 1)$ complex vector defined as

$$\mathbf{w}_s(\omega) = \mathbf{Q}_s^T(\omega)\mathbf{v}_s(\omega) \tag{16}$$

Equations (14–16) are the similar forms to Eqs. (7–9), and therefore the discussion about the vibroacoustic modes in structural mode form is analogous with that in elemental radiator form. The repetitive description is avoided here. The measurement system using the vibroacoustic modal filters and weighting filters is illustrated in Fig. 1b. In this regard, however, the terms of $\mathbf{v}_s(\omega)$, that is, the normal velocities of the structural modes, are measured by the structural modal filters, which consist of a number of discrete sensors [39] or a number of distributed sensors [40–42]. The advantage of the structural mode form is that a number of discrete sensors can be replaced by a number of distributed sensors, and the computation

labor for the vibroacoustic modal filters, as well as the structural modal filters, can be avoided by incorporating these filtering functions into the distributed sensors, that is, the smart sensors [40–43]. However, the smart sensors, which function as the vibroacoustic modal filters, are available only for the case in which the frequency dependence of the vibroacoustic modal filters is negligible. The disadvantage of the structural mode form is that knowledge about the structural modes, such as the natural frequencies and shapes, is necessary. In Sec. III.B, the frequency independent vibroacoustic modal filters are formulated for baffled structures in free space.

Moreover, the weighting factor plays a role in balancing the different orders of the magnitude. A proper weighting factor is set as

$$\alpha_s(\omega) = \frac{\text{trace}\{\mathbf{\Omega}_s(\omega)\}}{M} = \frac{\text{trace}\{\mathbf{R}_s(\omega)\}}{M} \tag{17}$$

The terms of $\mathbf{R}(\omega)$ are the dimensional quantities with units of kg/s in free space (kg in an enclosed space), as is clear from Eq. (3), and the terms of $\mathbf{R}_s(\omega)$ are the dimensional quantities with units of 1/s in free space (nondimensional quantities in an enclosed space), as is clear from Eq. (13) and the assumption that the shapes of the structural modes are normalized with respect to the halves of the modal masses. Hence, the weighting factor is a dimensional quantity with the unit of 1/s in free space (nondimensional quantity in an enclosed space).

Equations (13–16) indicate that the terms of $\mathbf{\Omega}_s(\omega)$ are proportional to the radiation efficiencies of the radiation modes, the columns of $\mathbf{\Psi}^T\mathbf{Q}_s(\omega)$ are the shapes of the radiation modes, and the terms of $\mathbf{w}_s(\omega)$ are the amplitudes of the radiation modes [29]. Therefore, the contributions of the vibroacoustic modes to the error criterion are the sum of the weighting factor and the values proportional to the radiation efficiencies of the radiation modes, and the shapes and amplitudes of the vibroacoustic modes are the same as those of the radiation modes.

III. Frequency Independent Vibroacoustic Modal Filters for Baffled Structures in Free Space

The vibroacoustic modal filters consist of higher order digital filters due to their frequency dependence and, therefore, the frequency dependence should be omitted in the implementation. The omission of frequency dependence should be validated for the respective acoustic fields, for example, baffled structures in free space, three-dimensional structures in free space, and three-dimensional structures in an enclosed space, because the frequency dependence is related to the acoustic transfer functions as shown in Eqs. (7) and (14). Baffled structures in free space as illustrated in Fig. 2 are addressed in this paper.

Frequency independent vibroacoustic modal filters are formulated for baffled structures in free space as follows: Sec. III.A, elemental radiator form; and Sec. III.B, structural mode form.

A. Elemental Radiator Form

It is assumed that the vibrating structure is embedded in an infinite baffle in free space, and the acoustic transfer functions are based on the Rayleigh integral. $\mathbf{R}(\omega)$ is then written as [29]

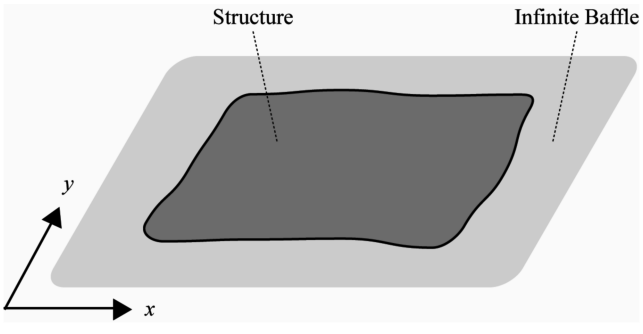

Fig. 2 Structure in an infinite baffle.

$$\mathbf{R}(\omega) = \frac{\omega^2\rho_0\Delta S^2}{4\pi c_0}\begin{bmatrix} 1 & \frac{\sin k|\mathbf{r}_1-\mathbf{r}_2|}{k|\mathbf{r}_1-\mathbf{r}_2|} & \cdots & \frac{\sin k|\mathbf{r}_1-\mathbf{r}_L|}{k|\mathbf{r}_1-\mathbf{r}_L|} \\ \frac{\sin k|\mathbf{r}_2-\mathbf{r}_1|}{k|\mathbf{r}_2-\mathbf{r}_1|} & 1 & \cdots & \frac{\sin k|\mathbf{r}_2-\mathbf{r}_L|}{k|\mathbf{r}_2-\mathbf{r}_L|} \\ \vdots & \vdots & \ddots & \vdots \\ \frac{\sin k|\mathbf{r}_L-\mathbf{r}_1|}{k|\mathbf{r}_L-\mathbf{r}_1|} & \frac{\sin k|\mathbf{r}_L-\mathbf{r}_2|}{k|\mathbf{r}_L-\mathbf{r}_2|} & \cdots & 1 \end{bmatrix} \tag{18}$$

where ΔS is the area of the elemental radiators, which is assumed to be constant; ρ_0 is the density of air; c_0 is the speed of sound in the air; $k(=\omega/c_0)$ is the wave number; and $\mathbf{r}_l$ is the representative location of the lth elemental radiator. Elliott and Johnson [29] calculated the eigenvectors of $\mathbf{R}(\omega)$, that is, the shapes of the radiation modes, for the beam and rectangular plate, and the calculation results indicated that if the nondimensional frequency is much smaller than unity, the eigenvectors of $\mathbf{R}(\omega)$ are approximately frequency independent. In this regard, however, the nondimensional frequency, that is, the nondimensional wave number, is defined as the ratio of the acoustic wave number to the structural wave number. In other words, the nondimensional frequency that is smaller than unity, let us say, lower nondimensional frequency, means that the size of the structure is smaller than the acoustic wavelength. Frequency independence is explained by the approximation of Eq. (18):

$$\mathbf{R}(\omega) \approx \frac{\omega^2\rho_0\Delta S^2}{4\pi c_0}\begin{bmatrix} 1 & 1 & \cdots & 1 \\ 1 & 1 & \cdots & 1 \\ \vdots & \vdots & \ddots & \vdots \\ 1 & 1 & \cdots & 1 \end{bmatrix} \tag{19}$$

and the assumption concerning the nondimensional frequency

$$k|\mathbf{r}_i - \mathbf{r}_j| \ll 1 \tag{20}$$

where subscripts i and j are $1, 2, 3, \ldots, L$, respectively. Equations (3) and (19) indicate that the contributions of all elemental radiators, as well as the couples to the acoustic power, are equal. Equation (19) indicates that, at lower nondimensional frequencies, the eigenvectors of $\mathbf{R}(\omega)$ are approximately frequency independent, whereas the terms of $\mathbf{R}(\omega)$ are proportional to the squared angular frequency and are still frequency dependent.

Furthermore, Eqs. (6) and (19) indicate that at lower nondimensional frequencies the eigenvectors of $\mathbf{R}_e(\omega)$ are approximately frequency independent, and thus, the amplitudes of the vibroacoustic modes can be approximately estimated by frequency independent vibroacoustic modal filters. Considering Eqs. (8), (9), and (19) together yields

$$J_{\text{vibroacoustic}}(\omega) \approx \mathbf{w}_e'^H(\omega)\mathbf{\Lambda}_e(\omega)\mathbf{w}_e'(\omega) \tag{21}$$

where $\mathbf{w}_e'(\omega)$ is the $(L \cdot 1)$ and complex vector defined as

$$\mathbf{w}_e'(\omega) = \mathbf{Q}_e^T\mathbf{v}_e(\omega) \tag{22}$$

and $\mathbf{Q}_e$ is $\mathbf{Q}_e(\omega)$ fixed with a certain lower nondimensional frequency at which Eq. (20) is satisfied. The columns of $\mathbf{Q}_e$ are the frequency independent vibroacoustic modal filters consisting of fixed gains rather than higher order digital filters. Figure 3a illustrates a measurement system using the frequency independent vibroacoustic modal filters and weighting filters. In Sec. IV.A, as a case study, the frequency independent vibroacoustic modal filters are applied to a baffled rectangular plate in free space.

Equations (6) and (19) indicate that at lower nondimensional frequencies, the rank of $\mathbf{R}_e(\omega)$ is approximately one, and this means that a single vibroacoustic mode contributes to the acoustic power. Further, Eq. (7) indicates that the single vibroacoustic mode has, as the contribution to the error criterion, the sum of $\alpha_e(\omega)$ and the single eigenvalue of $\mathbf{R}_e(\omega)$, and the other modes have, as equal contributions to the error criterion, $\alpha_e(\omega)$. It is then clear from Eq. (10) that the single vibroacoustic mode is much more contributive than the other modes.

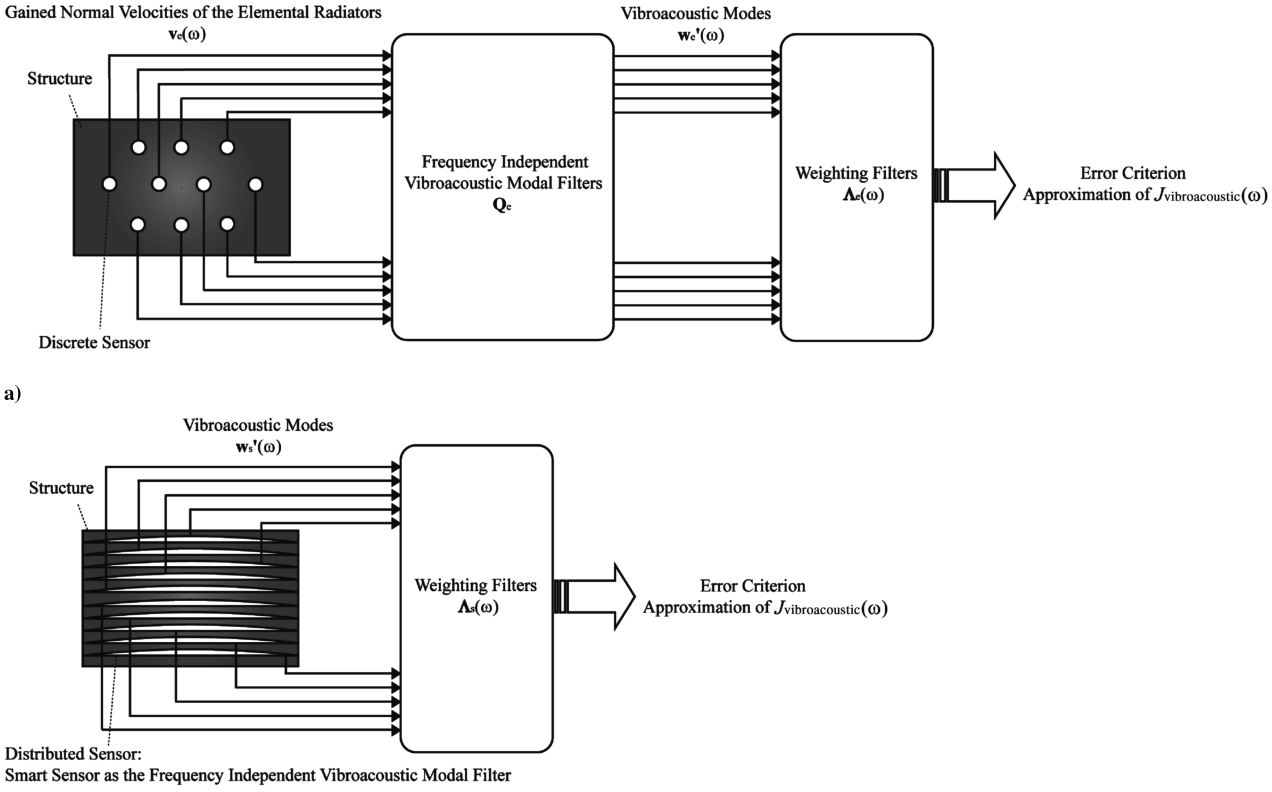

Fig. 3 Measurement systems using the frequency independent vibroacoustic modal filters and weighting filters for baffled structures in free space: a) elemental radiator form, and b) structural mode form.

B. Structural Mode Form

Equations (13) and (19) indicate that at lower nondimensional frequencies, the eigenvectors of $\mathbf{R}_s(\omega)$ are approximately frequency independent, and thus, the amplitudes of the vibroacoustic modes can be approximately estimated by the frequency independent vibroacoustic modal filters. Considering Eqs. (15), (16), and (19) together yields

$$J_{\text{vibroacoustic}}(\omega) \approx \mathbf{w}_s'^H(\omega)\mathbf{\Lambda}_s(\omega)\mathbf{w}_s'(\omega) \tag{23}$$

where $\mathbf{w}_s'(\omega)$ is the $(M \cdot 1)$ and complex vector defined as

$$\mathbf{w}_s'(\omega) = \mathbf{Q}_s^T\mathbf{v}_s(\omega) \tag{24}$$

and $\mathbf{Q}_s$ is $\mathbf{Q}_s(\omega)$ fixed with a certain lower nondimensional frequency at which Eq. (20) is satisfied. The columns of $\mathbf{Q}_s$ are the frequency independent vibroacoustic modal filters consisting of fixed gains rather than higher order digital filters. The smart sensors, which function as the frequency independent vibroacoustic modal filters, are available. Figure 3b illustrates a measurement system using the frequency independent vibroacoustic modal filters and weighting filters. In Sec. IV.B, as a case study, the frequency independent vibroacoustic modal filters are applied to a baffled rectangular plate in free space.

Equations (13) and (19) indicate that, at lower nondimensional frequencies, the rank of $\mathbf{R}_s(\omega)$ is approximately one, and this means that a single vibroacoustic mode contributes to the acoustic power. Further, Eq. (14) indicates that the single vibroacoustic mode has, as the contribution to the error criterion, the sum of $\alpha_s(\omega)$ and the single eigenvalue of $\mathbf{R}_s(\omega)$, and the other modes have, as equal contributions to the error criterion, $\alpha_s(\omega)$. It is then clear from Eq. (17) that the single vibroacoustic mode is much more contributive than the other modes.

IV. Case Study: Baffled Rectangular Plates in Free Space

The theories mentioned in the previous sections are applied to baffled rectangular plates in free space. In particular, the contributions of the vibroacoustic modes to the error criterion; the shapes of the vibroacoustic modes; the approximation error of the frequency independent vibroacoustic modal filters; the approximation error of the order reduction; and the structural kinetic energy and acoustic power, before and after optimal feedforward control, using the frequency independent vibroacoustic modal filters and order reduction, are simulated. Feedforward control is applicable only to the systems in which a coherent disturbance is available in advance of the control strategy, for example, propeller aircraft and helicopters; on the other hand, the feedback control is applicable to the case in which a coherent disturbance is not available in advance of the control strategy, for example, jet aircraft and rockets. The case study presented here is one of the preliminary investigations conducted to evaluate the validity and feasibility of the proposed theories.

The simulation results are presented and discussed as follows: Sec. IV.A, elemental radiator form; and Sec. IV.B, structural mode form.

A. Elemental Radiator Form

Figure 4 illustrates the system of interest, that is, a baffled and simply supported rectangular plate in free space. The x-directional length of the plate is 0.38 m; the y-directional length is 0.30 m; the thickness is 0.001 m; the Young's modulus is 71 GPa; the Poisson ratio is 0.33; the density of the half area, $0 \le x \le 0.19$ m, is 2720 kg/m^3; and the density of the other half area, $0.19 \le x \le 0.38$ m, is $1.1 \cdot 2720 = 2992$ kg/m^3. Because the masses of the elemental radiators are not uniform, the shapes and amplitudes of the vibroacoustic modes are different from those of the radiation modes, as mentioned in Sec. II.A. The anisotropic plate is

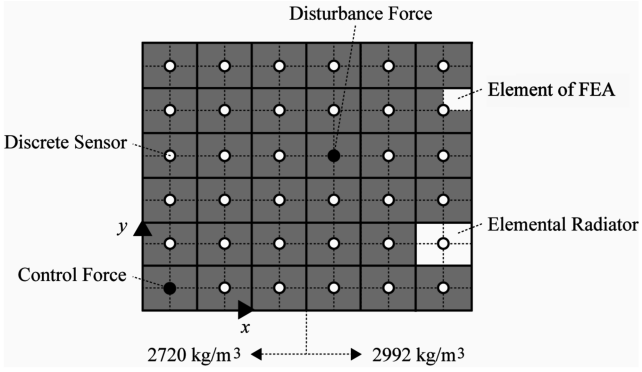

Fig. 4 Anisotropic rectangular plate with locations of discrete sensors, disturbance force, and control force.

modeled using the finite element method package ANSYS. The plate consists of 144 rectangular shell elements, and each elemental radiator consists of four rectangular shell elements. Therefore, the total number of elemental radiators is 36, and the center nodes of the individual elemental radiators are regarded as the representative locations. The total number of vibroacoustic modes is then 36, as is clear from Eq. (9). Moreover, the nondimensional frequency is defined as the wave number multiplied by the length of the plate [29], which is $k \cdot 0.38$ in this case.

Figure 5 shows the contributions of the first four vibroacoustic modes to the error criterion, that is, the largest four eigenvalues derived from Eq. (7): thin solid line, the first mode; thick solid line, the second mode; dashed line, the third mode; and dotted line, the fourth mode. The weighting factor is set as Eq. (10). The results are as follows: at lower nondimensional frequencies, $0 \leq k \cdot 0.38 < 1.0$, the contribution of the first mode is significant and the contributions of the other modes are almost equal, as expected in Eqs. (6), (7), and (19); at higher nondimensional frequencies, $1.0 \leq k \cdot 0.38 \leq 3.0$, the contribution of the first mode is still significant but the contributions of the other modes, especially the second and third modes, increase in relation to the nondimensional frequencies. It is suggested that for the entire range of nondimensional frequencies under consideration, $0 \leq k \cdot 0.38 \leq 3.0$, the error criterion can be approximated by the sum of the lower order vibroacoustic modes, and the order reduction is achievable where the modes increase with the nondimensional frequencies.

Figure 6 shows the shapes of the first vibroacoustic mode, that is, the eigenvectors derived from Eq. (7), with various nondimensional frequencies. The shapes are normalized with respect to the maximum value of the amplitude of the shape at the nondimensional frequency $k \cdot 0.38 = 0.25$. The shapes are the same as the vibroacoustic modal filters, as is clear from Eq. (9). In other words, Fig. 6 graphically shows the vibroacoustic modal filters for the first mode with various nondimensional frequencies. The results are as follows: at lower nondimensional frequencies, $0 \leq k \cdot 0.38 < 1.0$, the vibroacoustic modal filter for the first mode is approximately frequency independent, as expected from Eqs. (6) and (19); at higher nondimensional frequencies, $1.0 \leq k \cdot 0.38 \leq 3.0$, the vibroacoustic modal filter for the first mode is frequency dependent, as expected from Eqs. (6) and (18). This trend stays true to the vibroacoustic modal filters for higher modes, though the simulation results are not presented here because of space limitations. It is suggested that at lower nondimensional frequencies, $0 \leq k \cdot 0.38 < 1.0$, the amplitudes of the vibroacoustic modes can be approximately estimated by the frequency independent vibroacoustic modal filters.

Figure 7 shows the error criteria obtained in the following manners: solid line, the sum of all 36 vibroacoustic modes derived from Eq. (8), in which the emphasis is on using the (frequency dependent) vibroacoustic modal filters and not applying the order reduction; dashed line, the sum of all 36 vibroacoustic modes derived from Eq. (21), in which the emphasis is on using the frequency independent vibroacoustic modal filters with the fixed nondimensional frequency being $k \cdot 0.38 = 0.1$ and not applying the order reduction; and dotted line, the sum of the first nine vibroacoustic modes derived from Eq. (21), in which the emphasis is on using the frequency independent vibroacoustic modal filters with the fixed nondimensional frequency being $k \cdot 0.38 = 0.1$ and applying the order reduction. In all of the cases, the weighting factor is set as Eq. (10), the normal velocities at the representative locations of all 36 elemental radiators are assumed to be ideally measured (the dynamics of the discrete sensors are not modeled), and a disturbance shear force is applied at an arbitrarily chosen location ($7/12 \cdot 0.38$ m, $7/12 \cdot 0.30$ m), as illustrated in Fig. 4. The results from the comparison between the first two measurement systems are as follows: at lower nondimensional frequencies, $0 \leq k \cdot 0.38 < 1.0$, the approximation error of the frequency independent vibroacoustic modal filters is insignificant, as expected from Fig. 6; at higher nondimensional frequencies, $1.0 \leq k \cdot 0.38 \leq 3.0$, the approximation error is still insignificant. It is suggested that for the entire range of frequencies under consideration, $0 \leq k \cdot 0.38 \leq 3.0$, the amplitudes of the vibroacoustic modes can be approximately estimated by the frequency independent vibroacoustic modal filters. The results from the comparison between the last two measurement systems are as follows: at lower nondimensional frequencies, $0 \leq k \cdot 0.38 < 1.0$, the approximation error of the order reduction is insignificant, as expected from Fig. 5; at higher nondimensional frequencies, $1.0 \leq k \cdot 0.38 \leq 3.0$, the approximation error is significant, as was also expected from Fig. 5. In this regard, however, within the range of the nondimensional frequency,

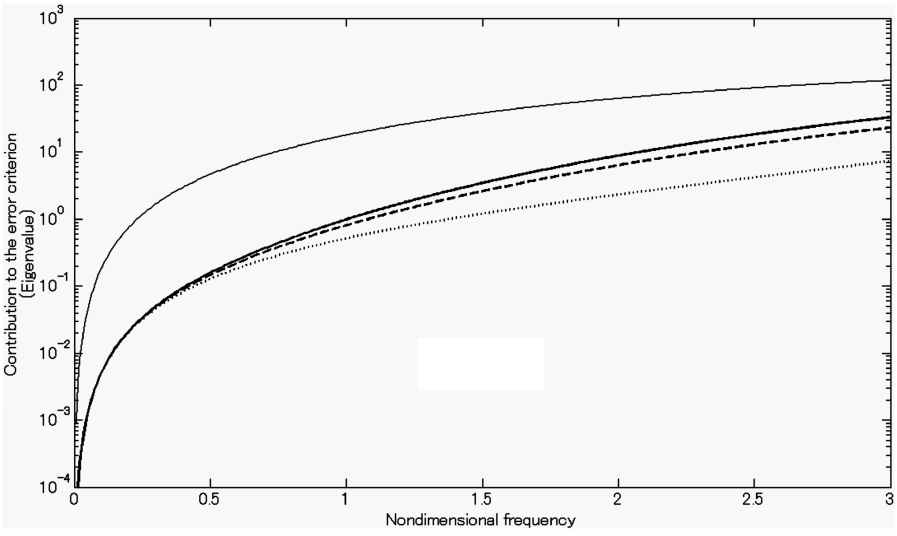

Fig. 5 Contributions of the first four vibroacoustic modes to the error criterion (the largest four eigenvalues).

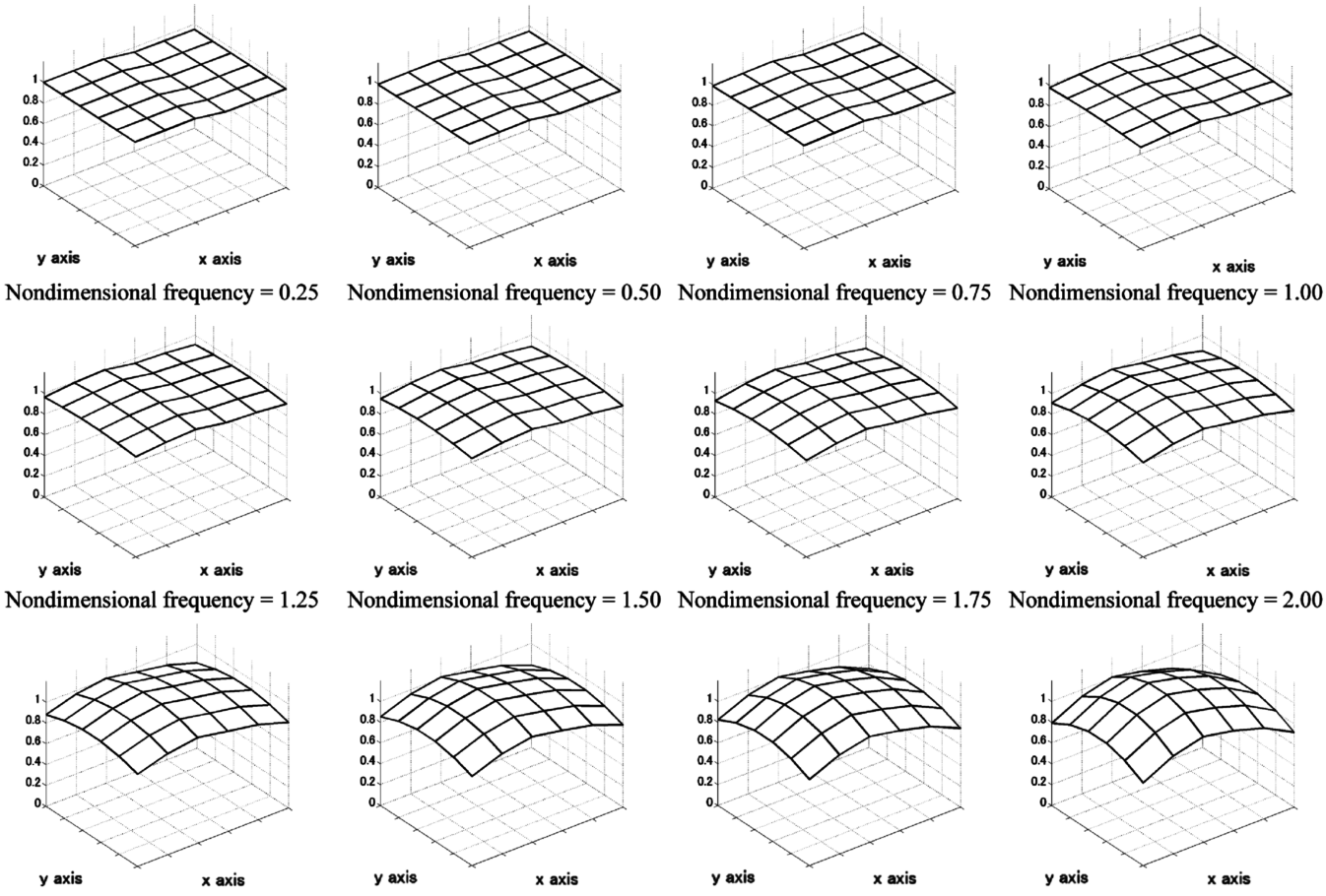

Fig. 6 Normalized shapes of the first vibroacoustic mode with various nondimensional frequencies.

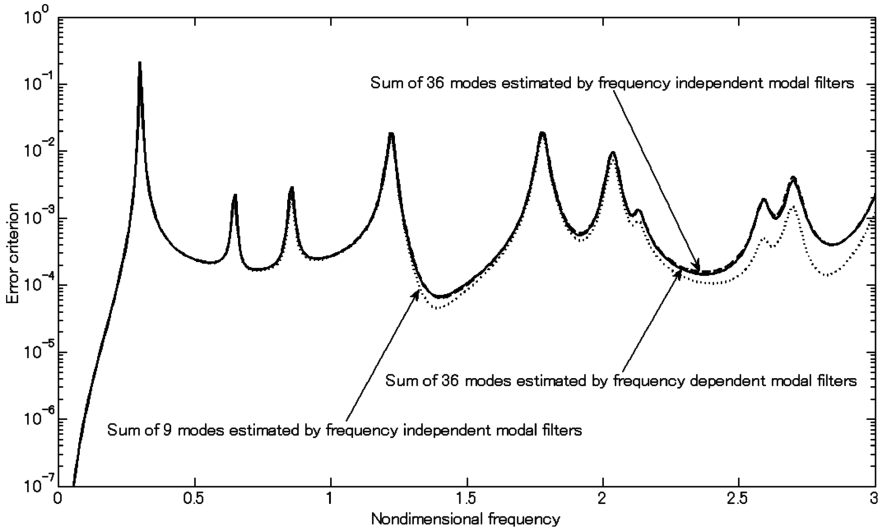

Fig. 7 Error criteria.

$1.0 \leq k \cdot 0.38 < 2.0$, the error criterion could still be approximated by the sum of the first nine vibroacoustic modes. Hence, it is suggested in this specific model that, within the range of the nondimensional frequency, $0 \leq k \cdot 0.38 < 2.0$, the error criterion can be approximated by the sum of the first nine vibroacoustic modes.

Figures 8 and 9 show the structural kinetic energy and acoustic power, both before and after optimal feedforward control, using the frequency independent vibroacoustic modal filters and weighting filters for the first nine modes. For this part of the study, the fixed nondimensional frequency was set to $k \cdot 0.38 = 0.1$ and the following weighting factors were used: thin solid line, without control; thick solid line, the weighting factor in Eq. (10), in which the emphasis is on controlling both vibration and sound; dashed line, at 100 times, in which the emphasis is on controlling vibrations; and dotted line, at 0.01 times, in which the emphasis is on controlling sound. The objective of this paper is to control both vibration and sound and, therefore, the first weighting factor is the main issue, whereas the others are just for comparison. The weighting factor does not affect the vibroacoustic modal filters, but affects the weighting

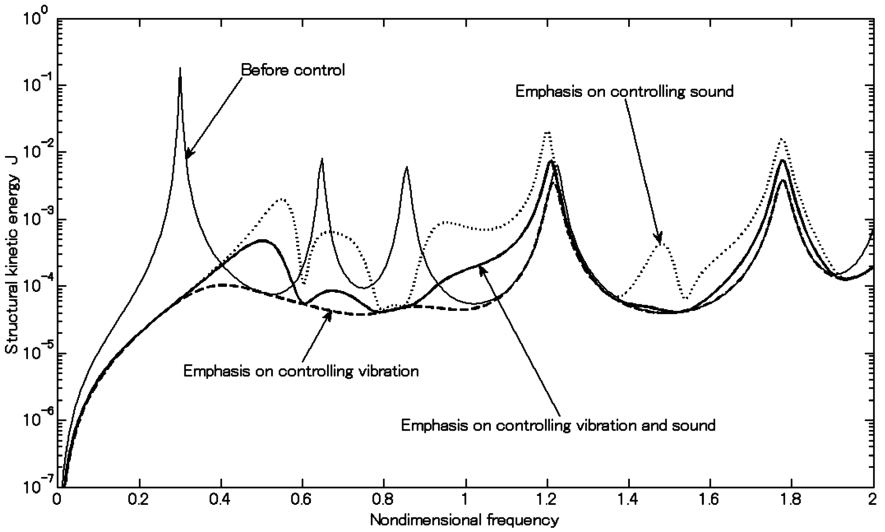

Fig. 8 Structural kinetic energy before and after optimal feedforward control using frequency independent vibroacoustic modal filters and weighting filters with the first nine modes.

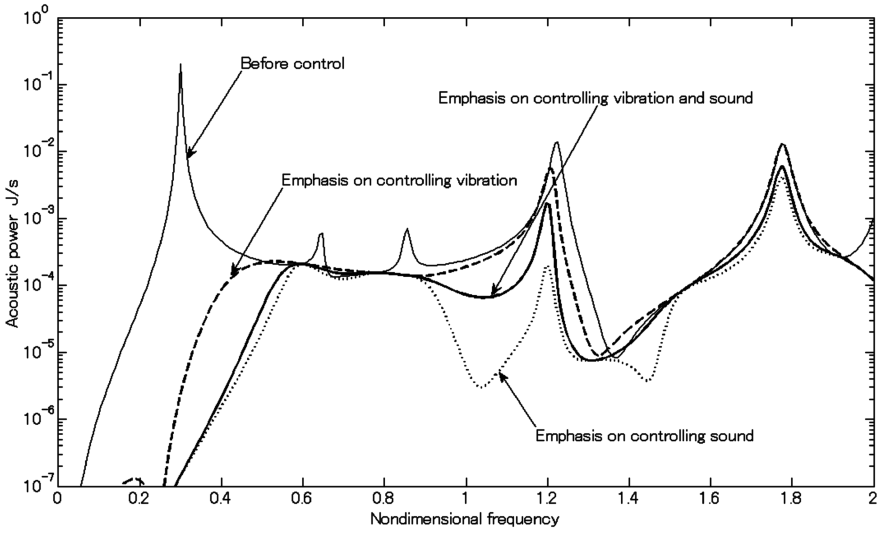

Fig. 9 Acoustic power before and after optimal feedforward control using frequency independent vibroacoustic modal filters and weighting filters with the first nine modes.

filters, as is clear from Eq. (7). In all of the cases, the normal velocities at the representative locations of all 36 elemental radiators are assumed to be ideally measured (the dynamics of the discrete sensors are not modeled), a disturbance shear force is applied at an arbitrarily chosen location ($7/12 \cdot 0.38$ m, $7/12 \cdot 0.30$ m), and a control shear force is applied at an arbitrarily chosen location ($1/12 \cdot 0.38$ m, $1/12 \cdot 0.30$ m), as illustrated in Fig. 4. The error criterion in Eq. (21) is minimized by conventional feedforward quadratic optimization [17] to derive the amplitude and phase of the control force. Nondimensional frequencies under control are $0 \leq k \cdot 0.38 \leq 2.0$, in accordance with the suggestion from Fig. 7. The results are as follows: in the dashed line, the weighting factor emphasizes controlling vibration at the expense of sound reduction and, therefore, this control strategy works best in Fig. 8; in the dotted line, the weighting factor emphasizes controlling sound at the expense of vibration reduction and, therefore, this control strategy works best in Fig. 9; and in the thick solid line, the weighting factor, which is the key objective of this paper, emphasizes controlling vibration and sound and, therefore, this control strategy serves as the best optimized choice for both Figs. 8 and 9. Thus, the thick solid line can be seen to be bounded by the dashed and dotted curves and, most importantly, shows a net reduction of both vibration and sound when compared with the thin solid line, which depicts the state before control. Furthermore, these simulation results imply the comparison between the conventional structural kinetic energy minimization corresponding to the dashed line, the conventional acoustic power minimization corresponding to the dotted line, and the proposed vibroacoustic control corresponding to the thick solid line.

B. Structural Mode Form

Figure 10 illustrates the system of interest, that is, a baffled and simply supported rectangular plate in free space. The x-directional length of the plate is 1.0 m, the y-directional length is 0.2 m, the thickness is 0.001 m, the Young's modulus is 71 GPa, the Poisson ratio is 0.33, the density is 2720 kg/m^3, the total of the x-directional structural modes is 12, and the total of the y-directional structural modes is 12. Therefore, the total number of structural modes is 144. However, only the 12 x-directional structural modes, (1,1), (1,2), (1,3), ..., and (1,12), are considered to simplify the design of the vibroacoustic modal and weighting filters. The total number of vibroacoustic modes is 12, as is clear from Eq. (16). The omission of the y-directional structural modes may be valid at lower frequencies due to the aspect ratio of the plate. In fact, it has been confirmed that there are no natural frequencies present at the y-directional structural modes for the entire range of nondimensional frequencies under consideration, $0 \leq k \cdot 1.0 \leq 3.0$. Again, the shapes and amplitudes of the vibroacoustic modes are the same as those of the radiation

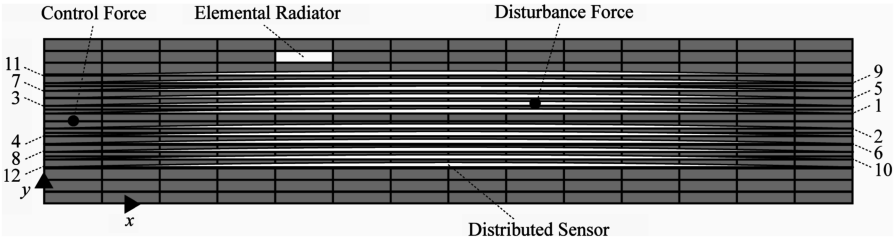

Fig. 10 Isotropic rectangular plate with locations of distributed sensors, disturbance force, and control force.

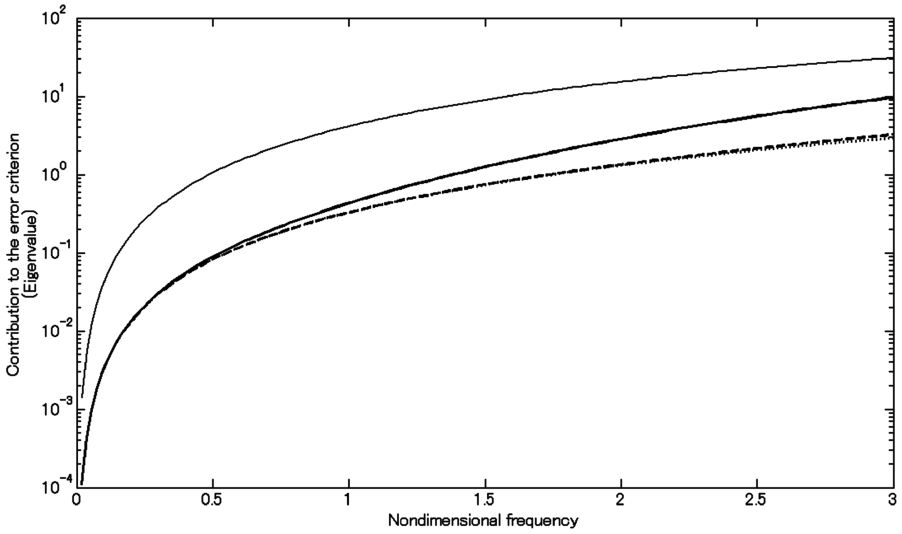

Fig. 11 Contributions of first four vibroacoustic modes to the error criterion (the largest four eigenvalues).

modes, as mentioned in Sec. II.B. The isotropic plate is modeled analytically [44]. There are a total of 196 elemental radiators, and the centers of the individual elemental radiators are regarded as the representative locations. In this regard, however, the elemental radiators are considered not to derive the vibroacoustic modes but to plot the shapes of the vibroacoustic modes, that is, the columns of $\mathbf{\Psi}^T\mathbf{Q}_s(\omega)$, as presented later in Fig. 12. Moreover, the nondimensional frequency is defined as the wave number multiplied by the length of the plate [29], which is $k \cdot 1.0$ in this case.

Figure 11 shows the contributions of the first four vibroacoustic modes to the error criterion, that is, the largest four eigenvalues derived from Eq. (14), in which only the 12 x-directional structural modes are considered: thin solid line, the first mode; thick solid line, the second mode; dashed line, the third mode; and dotted line, the fourth mode. The weighting factor is set as in Eq. (17). The results are as follows: at lower nondimensional frequencies, $0 \leq k \cdot 1.0 < 1.0$, the contribution of the first mode is significant and the contributions of the other modes are equal, as expected from Eqs. (13), (14), and (19); at higher nondimensional frequencies, $1.0 \leq k \cdot 1.0 \leq 3.0$, the contribution of the first mode is still significant but the contributions of the other modes, especially the second mode, increase in relation to the nondimensional frequencies. It is suggested that for the entire range of nondimensional frequencies under consideration, $0 \leq k \cdot 1.0 \leq 3.0$, the error criterion can be approximated by the sum of the lower order vibroacoustic modes, and the order reduction is achievable where the modes increase with the nondimensional frequencies.

Figure 12 shows the shapes of the first vibroacoustic mode, that is, the eigenvectors derived from Eq. (14), with various nondimensional frequencies, and in which only the 12 x-directional structural modes are considered. The shapes are normalized with respect to the maximum value of the amplitude of the shape at the nondimensional frequency $k \cdot 1.0 = 0.25$. The shapes of the vibroacoustic modes are the same as the vibroacoustic modal filters conjugated with the shapes of the structural modes, as is clear from Eq. (16). In other words, Fig. 12 graphically shows the vibroacoustic modal filters for the first mode with various nondimensional frequencies. The results are as follows: at lower nondimensional frequencies, $0 \leq k \cdot 1.0 < 1.0$, the vibroacoustic modal filter for the first mode is approximately frequency independent, as expected from Eqs. (13) and (19); at higher nondimensional frequencies, $1.0 \leq k \cdot 1.0 < 3.0$, the vibroacoustic modal filter for the first mode is frequency dependent, as expected from Eqs. (13) and (18). This trend remains true to the vibroacoustic modal filters for higher modes, though the simulation results are not presented here because of space limitations. It is suggested that at lower nondimensional frequencies, $0 \leq k \cdot 1.0 < 1.0$, the amplitudes of the vibroacoustic modes can be approximately estimated by the frequency independent vibroacoustic modal filters. In addition, if more structural modes were considered for the derivation of the vibroacoustic modes, smoother shapes of the vibroacoustic modes could be obtained.

Figure 13 shows the error criteria obtained in the following manners: solid line, the sum of all 12 vibroacoustic modes derived from Eq. (15), in which the emphasis is on using the (frequency dependent) vibroacoustic modal filters and not applying the order reduction; dashed line, the sum of all 12 vibroacoustic modes derived from Eq. (23), in which the emphasis is on using the frequency independent vibroacoustic modal filters with the fixed nondimensional frequency being $k \cdot 0.38 = 0.1$ and not applying the order reduction; and dotted line, the sum of the first six vibroacoustic modes derived from Eq. (23), in which the emphasis is on using the frequency independent vibroacoustic modal filters with the fixed nondimensional frequency being $k \cdot 0.38 = 0.1$ and applying the order reduction. In all of the cases, only the 12 x-directional structural modes are considered for the derivation of the vibroacoustic modal filters and weighting filters. The weighting factor is set as Eq. (17); the normal velocities at the representative locations of all 36 elemental radiators are assumed to be ideally measured (the dynamics of the discrete sensors are not modeled); groups of 12 or 6 distributed sensors made of polyvinylidene fluoride (PVDF) are used; and a disturbance shear force is applied at an arbitrarily chosen location ($17/28 \cdot 1.0$ m, $17/28 \cdot 0.20$ m), as illustrated in Fig. 10. In

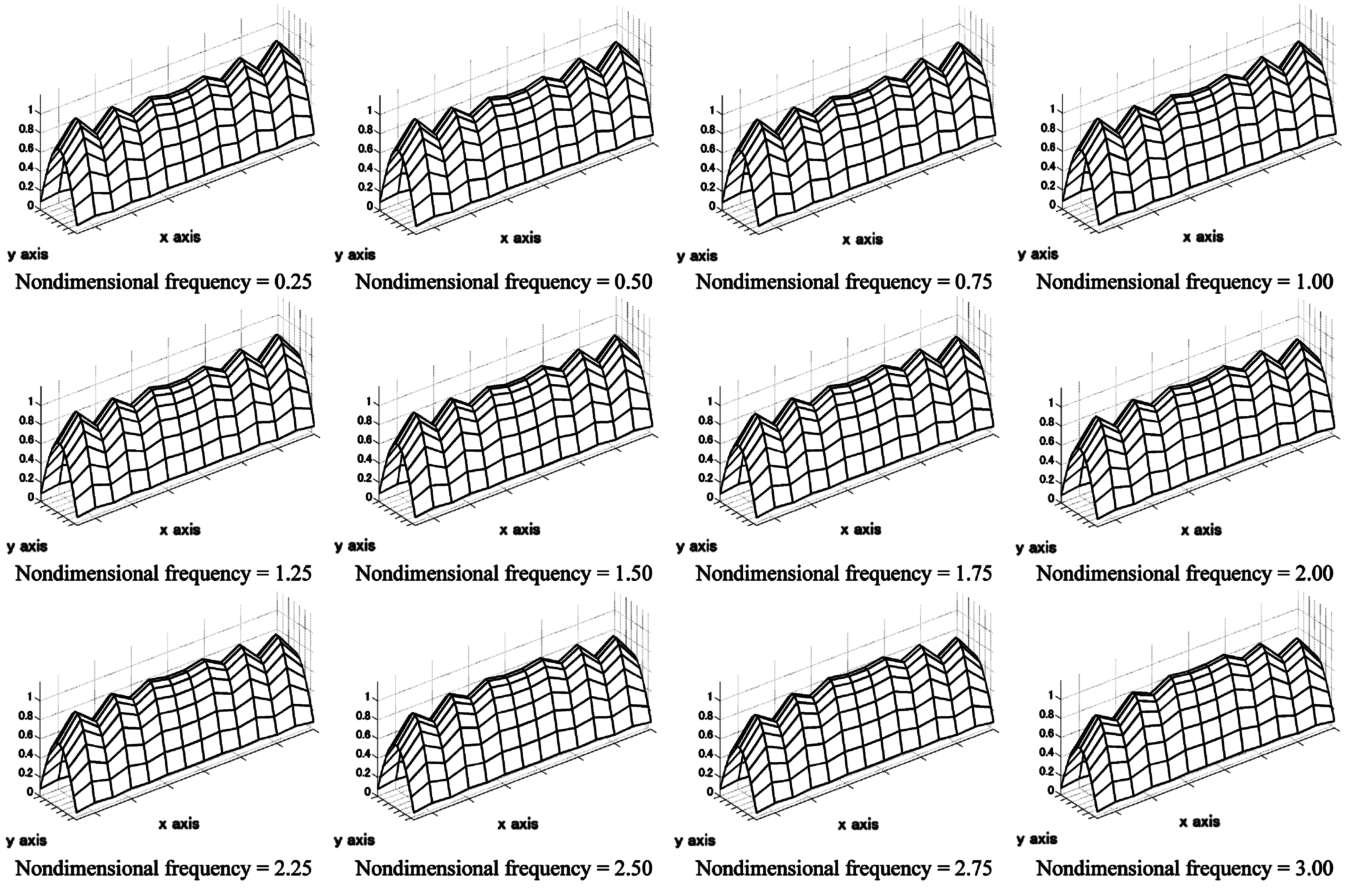

Fig. 12 Normalized shapes of the first vibroacoustic mode with various nondimensional frequencies.

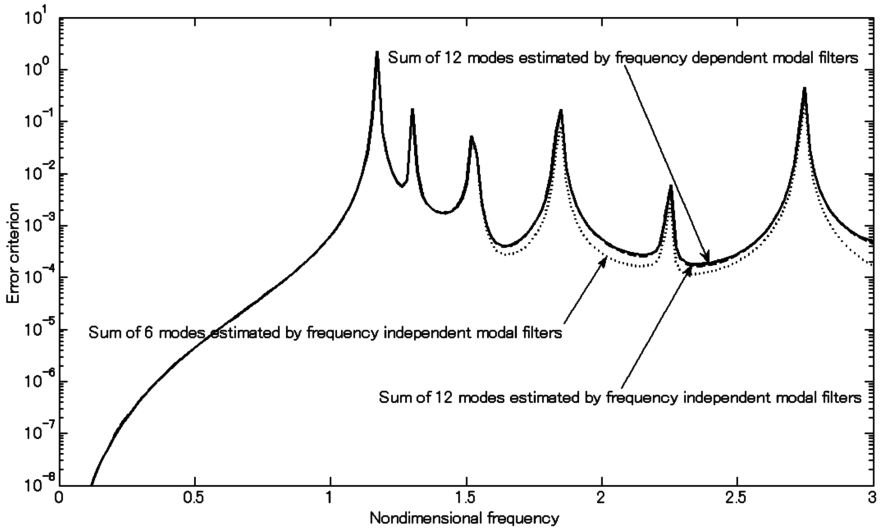

Fig. 13 Error criteria.

the following paragraphs, the configurations of the aforementioned measurement systems are stated in more detail.

The error criterion, estimated by the (frequency dependent) vibroacoustic modal filters, is derived from

$$J_{\text{vibroacoustic}}(\omega) \approx \mathbf{w}_s''^H(\omega)\mathbf{\Lambda}_s(\omega)\mathbf{w}_s''(\omega) \tag{25}$$

where $\mathbf{w}_s''(\omega)$ is the $(M \cdot 1)$ and complex vector defined as

$$\mathbf{w}_s''(\omega) = j\omega\mathbf{Q}_s^T(\omega)\mathbf{q}(\omega) \tag{26}$$

and $j\omega\mathbf{q}(\omega)$ is the $(M \cdot 1)$ and complex vector, whose terms are the time-differentiated output charges of the PVDF smart sensors, which function as the structural modal filters. The 12 smart sensors are mounted along the x-direction, at $y = L_y/2 + 0.01$ m, $L_y/2 - 0.01$ m, $L_y/2 + 0.02$ m, $L_y/2 - 0.02$ m, $L_y/2 + 0.03$ m, $L_y/2 - 0.03$ m, $L_y/2 + 0.04$ m, $L_y/2 - 0.04m$, $L_y/2 + 0.05$ m, $L_y/2 - 0.05$ m, $L_y/2 + 0.06$ m, and $L_y/2 - 0.06$ m. The widths are varied according to some shaping functions, as illustrated in Fig. 10, to measure the normal velocities of all 12 x-directional structural modes. The numbers of smart sensors in the figure denotes the correspondence to the associated x-directional structural modes, from (1,1) to (12,1). However, the shapes of the smart sensors in the figure are not the actual ones, but their images. The shapes, thicknesses, and material properties of the smart sensors are detailed

in the Appendix, and the time-differentiated output charges are formulated in Eq. (A7).

The error criterion estimated by the frequency independent vibroacoustic modal filters is derived from

$$J_{\text{vibroacoustic}}(\omega) \approx \mathbf{w}_s'''^H(\omega)\mathbf{\Lambda}_s(\omega)\mathbf{w}_s'''(\omega) \tag{27}$$

where $\mathbf{w}_s'''(\omega)$ is the $(M \cdot 1)$ and complex vector defined as

$$\mathbf{w}_s'''(\omega) = j\omega\mathbf{q}'(\omega) \tag{28}$$

Here, $j\omega\mathbf{q}'(\omega)$ is the $(M \cdot 1)$ and complex vector, whose terms are the time-differentiated output charges of the PVDF smart sensors, which function as the frequency independent vibroacoustic modal filters. For the case without order reduction, 12 smart sensors are mounted along the x direction, at $y = L_y/2 + 0.01$ m, $L_y/2 - 0.01$ m, $L_y/2 + 0.02$ m, $L_y/2 - 0.02$ m, $L_y/2 + 0.03$ m, $L_y/2 - 0.03$ m, $L_y/2 + 0.04$ m, $L_y/2 - 0.04$ m, $L_y/2 + 0.05$ m, $L_y/2 - 0.05$ m, $L_y/2 + 0.06$ m, and $L_y/2 - 0.06$ m. As before, the widths are varied according to some shaping functions, as illustrated in Fig. 10, to measure the amplitudes of all 12 vibroacoustic modes. For the case with the order reduction, the six smart sensors are mounted along the x direction, at $y = L_y/2 + 0.01$ m, $L_y/2 - 0.01$ m, $L_y/2 + 0.02$ m, $L_y/2 - 0.02$ m, $L_y/2 + 0.03$ m, and $L_y/2 - 0.03$ m, with the widths varied according to some shaping functions, as illustrated in Fig. 10, to measure the amplitudes of the first six vibroacoustic modes. The number of the smart sensors in the figure denotes the correspondence to the associated vibroacoustic modes, from the first to the sixth. Again, the shapes of the smart sensors in the figure are not the actual ones, but their images. The shapes, thicknesses, and material properties of the smart sensors are detailed in the Appendix, and the time-differentiated output charges are formulated in Eq. (A10).

The results from the comparison between the first two measurement systems are as follows: at lower nondimensional frequencies, $0 \le k \cdot 1.0 < 1.0$, the approximation error of the frequency independent vibroacoustic modal filters is insignificant, as expected from Fig. 12; at higher nondimensional frequencies, $1.0 \le k \cdot 1.0 \le 3.0$, the approximation error is still insignificant. It is suggested that for the entire range of nondimensional frequencies under consideration, $0 \le k \cdot 1.0 \le 3.0$, the amplitudes of the vibroacoustic modes can be approximately estimated by the frequency independent vibroacoustic modal filters. The results from the comparison between the last two measurement systems are as follows: at lower nondimensional frequencies, $0 \le k \cdot 1.0 < 1.0$, the approximation error of the order reduction is insignificant, as expected from Fig. 11; at higher nondimensional frequencies, $1.0 \le k \cdot 1.0 < 3.0$, the approximation error is more significant, as was also expected from Fig. 11. In this regard, however, within the range of the nondimensional frequency, $1 \le k \cdot 1.0 < 1.5$, the error criterion could still be approximated by the sum of the first six vibroacoustic modes. Hence, it is suggested in this specific model that within the range of the nondimensional frequency, $0 \le k \cdot 1.0 < 1.5$, the error criterion can be approximated by the sum of the first six vibroacoustic modes.

Figures 14 and 15 show the structural kinetic energy and acoustic power, both before and after optimal feedforward control, using the frequency independent vibroacoustic modal filters and weighting filters for the first six modes. In this part of the study, the fixed nondimensional frequency was set to $k \cdot 1.0 = 0.1$ and the following weighting factors were employed: thin solid line, without control; thick solid line, the weighting factor in Eq. (17), in which the emphasis is on controlling both vibration and sound; dashed line, at 100 times, in which the emphasis is on controlling vibrations; and dotted line, at 0.01 times, in which the emphasis is on controlling sound. The objective of this paper is to control both vibration and sound, and therefore the first weighting factor is the main issue, whereas the others are just for comparison. The weighting factor does not affect the vibroacoustic modal filters but affects the weighting filters, as is clear from Eq. (14). In all of the cases, a disturbance shear force is applied at an arbitrarily chosen location ($17/28 \cdot 1.0$ m, $17/28 \cdot 0.2$ m), and a control shear force is also applied at an arbitrarily chosen location ($1/28 \cdot 1.0$ m, $1/2 \cdot 0.2$ m), as illustrated in Fig. 10. The error criterion in Eq. (27) is minimized by conventional feedforward quadratic optimization [17] to derive the amplitude and phase of the control force. Nondimensional frequencies under control are $0 \le k \cdot 1.0 < 1.5$, in accordance with Fig. 13. The results are as follows: in the dashed line, the weighting factor emphasizes controlling vibration at the expense of sound reduction and, therefore, this control strategy works best in Fig. 14; in the dotted line, the weighting factor emphasizes controlling sound at the expense of vibration reduction and, therefore, this control strategy works best in Fig. 15; and in the thick solid line, the weighting factor, which is the key objective of this paper, emphasizes controlling vibration and sound and, therefore, this control strategy serves as the best optimized choice for both Figs. 14 and 15. Thus, the thick solid line can be seen to be bounded by the dashed and dotted curves and, most importantly, shows a net reduction of both vibration and sound when compared with the thin solid line, which depicts the state before control. Furthermore, these simulation results imply the comparison between the conventional structural kinetic energy minimization corresponding to dashed line, the conventional acoustic power minimization corresponding to dotted line, and the proposed vibroacoustic control corresponding to thick solid line.

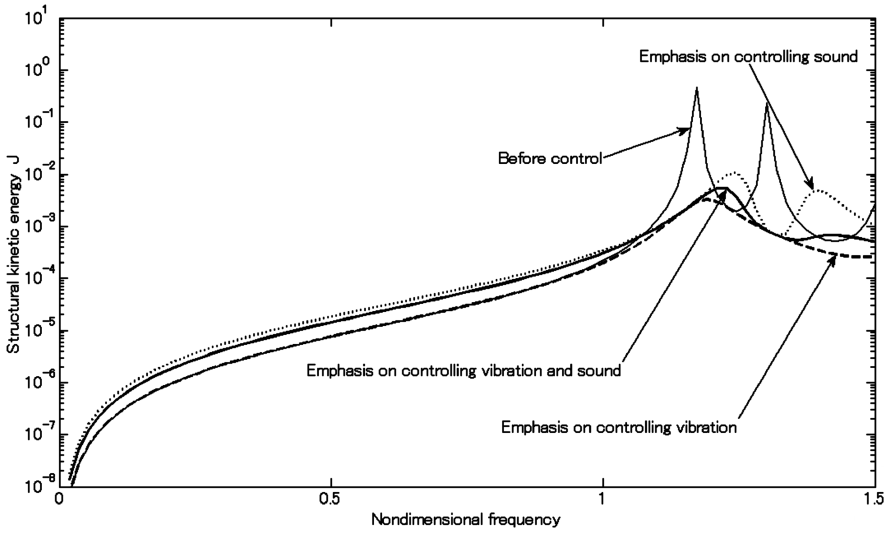

Fig. 14 Structural kinetic energy before and after optimal feedforward control using the frequency independent vibroacoustic modal filters and weighting filters with the first six modes.

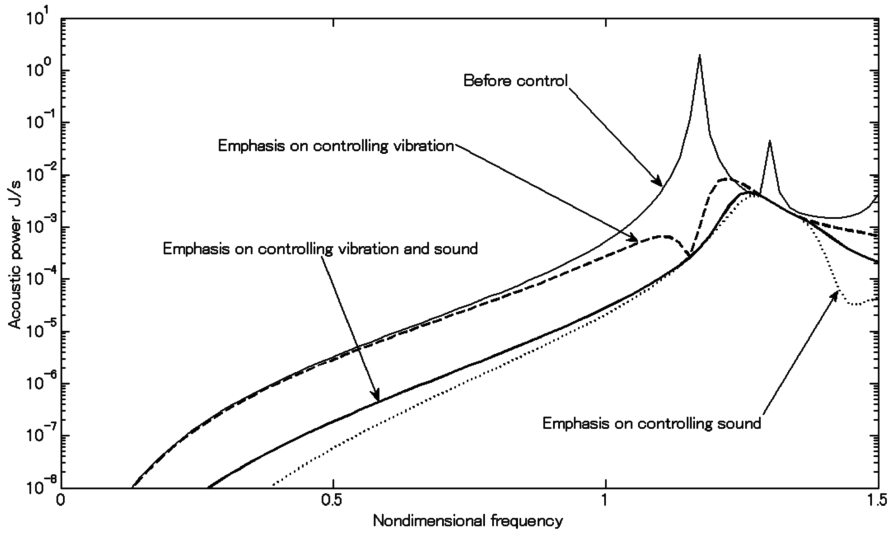

Fig. 15 Acoustic power before and after optimal feedforward control using the frequency independent vibroacoustic modal filters and weighting filters with the first six modes.

V. Conclusions

For the purpose of controlling both vibration and sound, the orthogonal contributors with respect to the sum of the structural kinetic energy and acoustic power in free space (acoustic potential energy in enclosed space), termed vibroacoustic modes, have been formulated in two ways: an elemental radiator form and a structural mode form. Like the structural and radiation modes, the vibroacoustic modes have both eigenvalues and eigenvectors. The eigenvalues imply the contributions of the vibroacoustic modes to the sum of the structural kinetic energy and acoustic power (acoustic potential energy), and the eigenvectors imply the shapes of the vibroacoustic modes.

Frequency dependent spatial filters, which can estimate the amplitudes of the vibroacoustic modes, termed vibroacoustic modal filters, have been formulated in both elemental radiator and structural mode forms. In the elemental radiator form, the vibroacoustic modal filters are derived from the masses of the elemental radiators and the acoustic transfer functions between the elemental radiators. In addition, the amplitudes of the vibroacoustic modes are estimated by passing the measured normal velocities of the elemental radiators to the vibroacoustic modal filters. The advantage of this form is that no prior knowledge about the structural modes is necessary. The disadvantage is that a number of discrete sensors are required and, therefore, an increase in computation labor for the vibroacoustic modal filters is inevitable. In the structural mode form, the vibroacoustic modal filters are derived from the shapes of the structural modes and the acoustic transfer functions between the structural modes. Then, the amplitudes of the vibroacoustic modes are estimated by passing the measured normal velocities of the structural modes to the vibroacoustic modal filters. The advantage of this form is that a number of discrete sensors can be replaced with distributed sensors. Thus, the computation labor for the vibroacoustic modal filters, as well as for the structural modal filters, can be avoided by incorporating these filtering functions into the distributed sensors, that is, the smart sensors. However, the smart sensors, which function as the vibroacoustic modal filters, are available only in the cases in which the frequency dependence is negligible. The disadvantage is that knowledge about the structural modes, such as the natural frequencies and shapes, is necessary. One of the two forms should be used selectively according to the situation; in both forms, the frequency dependence of the vibroacoustic modal filters is a common difficulty faced during implementation.

Frequency independent vibroacoustic modal filters have been formulated for baffled structures in free space, in both elemental radiator and structural mode forms. This approach is based on specific characteristics, whereby for baffled structures in free space, the frequency dependence of vibroacoustic modal filters is negligible at lower nondimensional frequencies.

The developed theories have been applied to an optimal feedforward control system for baffled rectangular plates in free space, which is excited by a disturbance shear force, and the performance has been demonstrated through numerical simulations in both forms. In the elemental radiator form, 36 ideal discrete sensors (the dynamics of these sensors are not considered in the simulation) have been used to measure the normal velocities of the elemental radiators, and these measured velocities have been passed into the frequency independent vibroacoustic modal filters consisting of 36 input and 9 output fixed gains to estimate the amplitudes of the most contributive nine modes. Following the order reduction, the sum of the structural kinetic energy and acoustic power has been successfully regulated by a control shear force at lower nondimensional frequencies. In the structural mode form, six smart sensors made of PVDF have been used to directly estimate the amplitudes of the most contributive six modes and, subsequently, the computation labor for the vibroacoustic modal filters, as well as for the structural modal filters, has been completely avoided. Following the order reduction, the sum of the structural kinetic energy and acoustic power has been successfully regulated by a control shear force at lower nondimensional frequencies.

Some future tasks are mentioned hereinafter. First, the frequency dependence of the vibroacoustic modal filters for three-dimensional structures in free space and enclosed space must be investigated to explore the applicability of the frequency independent vibroacoustic modal filters to real aerospace vehicles. Although the disturbance input for the simulation model in this paper is a shear force for simplicity, reality in the aerospace vehicles is different. For example, the aircraft fuselage is excited by a turbulent boundary layer (TBL) [2,7,9] and the acoustic pressure generated from the propeller and jet engines, and the space rocket is excited by the TBL and the acoustic pressure originally generated from the jet engine and then reflected by the ground during launch. The simulation including the physics of the TBL and the acoustic pressure around the aircraft vehicles must be conducted to predict more realistic control performance and, furthermore, the experimental verification must be carried out by wind tunnel, measured data of the acoustic pressure, and flight test. Second, though the control input for the simulation in this paper is a shear force, reality is different. For instance, lead, zirconate, and titanate (PZT) patches could be employed as the control actuators in practice because of their low profile and lightweight property. However, because PZT actuators have a number of drawbacks, for example, the requirement of high-voltage amplifiers, harmonic distortion, limited actuation strength at low frequencies, and brittleness, electric actuators such as a proof-mass actuator [34] and distributed active vibration absorber [11] could be an alternative in

spite of their relatively larger weights. All of these actuators do not generate a pure shear force and do couple with the structure and, therefore, the simulation including the physics of the actuators and the experimental verification must be performed.

Appendix

Smart sensors made of distributed piezoelectric materials are designed in either one-dimensional [40,41,43] or two-dimensional forms [42]. In the one-dimensional design, the widths of the piezoelectric materials are shaped. In the two-dimensional design, it is the thickness of the material that is shaped. Although two-dimensional smart sensors are ideal for structures, such as the rectangular plate used in Sec. IV.B, shaping the thickness is not easy in practice. Consequently, one-dimensional smart sensors were employed in this paper.

Normal velocity of a plate $v(x, y, \omega)$ is written as

$$v(x, y, \omega) = \sum_{m_x=1}^{M_x} \sum_{m_y=1}^{M_y} \psi_{m_x m_y}(x, y) v_{m_x m_y}(\omega) \tag{A1}$$

where m_x is the index of the x-directional structural mode, m_y is the index of the y-directional structural mode, $\psi_{mxmy}(x, y)$ is the shape, and $v_{mxmy}(\omega)$ is the normal velocity. If the plate is isotropic, rectangular, and simply supported, the shape of the structural mode is written as [44]

$$\psi_{m_x m_y}(x, y) = \sqrt{\frac{8}{\rho_s h_s L_x L_y}} \sin\frac{m_x \pi}{L_x} x \sin\frac{m_y \pi}{L_y} y \tag{A2}$$

where L_x is the x-directional length of the plate, L_y is the y-directional length, h_s is the thickness, ρ_s is the density, and the shape of the structural mode is normalized with respect to half of the modal mass. Moreover, the normal velocity of the structural mode is written as [44]

$$v_{m_x m_y}(\omega) = \frac{j\omega}{\omega_{m_x m_y}^2 - \omega^2 + j\eta_{m_x m_y}\omega_{m_x m_y}\omega} \sqrt{\frac{2}{\rho_s h_s L_x L_y}} f \sin\frac{m_x \pi}{L_x} x_f \sin\frac{m_y \pi}{L_y} y_f \tag{A3}$$

where ω_{mxmy} is the natural frequency of the structural mode, η_{mxmy} is the damping ratio, f is the complex amplitude of the external force, and x_f and y_f are the locations of the force in the x and y directions.

With the aim of developing a smart sensor, which functions as the structural modal filter for the x-directional mode, a distributed sensor made of PVDF is mounted on the plate along the x direction, at $y = y_0$, with the width varied according to the shaping function $\Gamma(x)$, as shown in Fig. A1. The time-differentiated output charge of the distributed sensor $j\omega q(\omega)$ is then written as [40]

$$j\omega q(\omega) = \frac{h_p + h_s}{2} \int_{y_0}^{y_0+\Gamma(x)} \int_0^{L_x} \left\{ e_{31} \frac{\partial^2 v(x, y, \omega)}{\partial x^2} + e_{32} \frac{\partial^2 v(x, y, \omega)}{\partial y^2} \right\} \mathrm{d}x\, \mathrm{d}y \tag{A4}$$

where h_p is the thickness of the PVDF, e_{31} is the x-directional piezoelectric field intensity constant, and e_{32} is the y-directional piezoelectric field intensity constant. In accordance with the work by Tanaka et al. [41], the shaping function for the m_xth structural mode is designed as

$$\Gamma(x) = \Gamma_{m_x}(x) = \frac{A_{m_x}}{\{e_{31}(\frac{m_x\pi}{L_x})^2 + e_{32}(\frac{\pi}{L_y})^2\} \sin\frac{\pi}{L_y} y_0} \sin\frac{m_x \pi}{L_x} x \tag{A5}$$

where A_{mx} is the real factor that satisfies

$$A_{m_x} \ll \sin\frac{\pi}{L_y} y_0 \left\{ e_{31} \left(\frac{m_x \pi}{L_x}\right)^2 + e_{32} \left(\frac{\pi}{L_y}\right)^2 \right\} \tag{A6}$$

Substituting Eq. (A5) into Eq. (A4) yields

$$j\omega q(\omega) \approx \sqrt{\frac{L_x}{2\rho_s h_s L_y}} (h_p + h_s) A_{m_x} \sum_{m_y=1}^{M_y} v_{m_x m_y} \times \frac{e_{31}(\frac{m_x\pi}{L_x})^2 + e_{32}(\frac{m_y\pi}{L_y})^2}{e_{31}(\frac{m_x\pi}{L_x})^2 + e_{32}(\frac{\pi}{L_y})^2} \frac{\sin\frac{m_y\pi}{L_y} y_0}{\sin\frac{\pi}{L_y} y_0} \tag{A7}$$

Equation (A7) indicates that the time-differentiated output charge includes only the normal velocities of the m_xth structural modes. The y-directional structural modes may be negligible at lower frequencies due to the aspect ratio of the plate. Equation (A7) is then approximated as

$$j\omega q(\omega) \approx \sqrt{\frac{L_x}{2\rho_s h_s L_y}} (h_p + h_s) A_{m_x} v_{m_x 1} \tag{A8}$$

Equation (A8) indicates that the time-differentiated output charge is proportional to the normal velocity of the $(m_x, 1)$ structural mode.

Next, with the aim of developing a smart sensor, which functions as the vibroacoustic modal filter, the shaping function for the nth vibroacoustic mode is designed as

$$\Gamma(x) = \Gamma_n(x) = \sum_{m_x=1}^{M_x} Q_{nm_x} \Gamma_{m_x}(x) = \frac{1}{\sin\frac{\pi}{L_y} y_0} \sum_{m_x=1}^{M_x} \frac{Q_{nm_x} A_{m_x}}{e_{31}(\frac{m_x\pi}{L_x})^2 + e_{32}(\frac{\pi}{L_y})^2} \sin\frac{m_x \pi}{L_x} x \tag{A9}$$

where Q_{nmx} is the m_xth term of the nth column of $\mathbf{Q}_s$. Substituting Eq. (A9) into Eq. (A4) yields

$$j\omega q(\omega) \approx \sqrt{\frac{L_x}{2\rho_s h_s L_y}} (h_p + h_s) \sum_{m_x=1}^{M_x} \sum_{m_y=1}^{M_y} Q_{nm_x} A_{m_x} v_{m_x m_y} \times \frac{e_{31}(\frac{m_x\pi}{L_x})^2 + e_{32}(\frac{m_y\pi}{L_y})^2}{e_{31}(\frac{m_x\pi}{L_x})^2 + e_{32}(\frac{\pi}{L_y})^2} \frac{\sin\frac{m_y\pi}{L_y} y_0}{\sin\frac{\pi}{L_y} y_0} \tag{A10}$$

The y-directional structural modes may be negligible at lower frequencies due to the aspect ratio of the plate. Equation (A10) is then approximated as

$$j\omega q(\omega) \approx (h_p + h_s) \sqrt{\frac{L_x}{2\rho_s h_s L_y}} \sum_{m_x=1}^{M_x} Q_{nm_x} A_{m_x} v_{m_x 1} \tag{A11}$$

Equation (A11) indicates that the time-differentiated output charge is proportional to the amplitude of the nth vibroacoustic mode.

In the simulations described in Sec. IV.B, the thickness of the PVDF is 0.0001 m, the x-directional piezoelectric field intensity constant is 0.0105 $\mathrm{C/m^2}$, the y-directional piezoelectric field intensity constant is 0.00035 $\mathrm{C/m^2}$, and A_{mx} is 0.001. In Fig. 13, the time-differentiated output charges are divided by $(L_x/2/\rho_s/h_s/L_y)^{1/2}(h_p + h_s)A_{mx}$ to tune the magnitudes to the normal velocities of the structural modes.

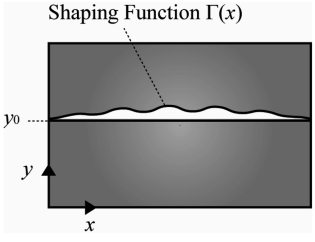

Fig. A1 The smart sensors made of PVDF on the plate.

Acknowledgment

The work was supported by the Japan Society for the Promotion of Science.

References

[1] Carneal, J. P., and Fuller, C. R., "Active Structural Acoustic Control of Noise Transmission through Double Panel Systems," *AIAA Journal*, Vol. 33, No. 4, 1995, pp. 618–623.

[2] Frampton, K. D., Clark, R. L., and Dowell, E. H., "State-Space Modeling for Aeroelastic Panels with Linearized Potential Flow Aerodynamic Loading," *Journal of Aircraft*, Vol. 33, No. 4, 1996, pp. 816–822.

[3] Varadan, V. V., Kim, J., and Varadan, V. K., "Optimal Placement of Piezoelectric Actuators for Active Noise Control," *AIAA Journal*, Vol. 35, No. 3, 1997, pp. 526–533.

[4] Grewal, A., Nitzsche, F., and Zimcik, D. G., "Active Control of Aircraft Cabin Noise Using Collocated Structural Actuators and Sensors," *Journal of Aircraft*, Vol. 35, No. 2, 1998, pp. 324–331.

[5] Gardonio, P., and Elliott, S. J., "Active Control of Structure-Borne and Airborne Sound Transmission Through Double Panel," *Journal of Aircraft*, Vol. 36, No. 6, 1999, pp. 1023–1033.

[6] Palumbo, D., Cabell, R., and Sullivan, B., "Flight Test of Active Structural Acoustic Noise Control System," *Journal of Aircraft*, Vol. 38, No. 2, 2001, pp. 277–285.

[7] Maury, C., Gardonio, P., and Elliott, S. J., "Active Control of the Flow-Induced Noise Transmitted Through a Panel," *Journal of Aircraft*, Vol. 38, No. 10, 2001, pp. 1860–1867.

[8] Gardonio, P., "Review of Active Techniques for Aerospace Vibro-Acoustic Control," *Journal of Aircraft*, Vol. 39, No. 2, 2002, pp. 206–214.

[9] Gibbs, G. P., Cabell, R. H., and Juang, J.-N., "Controller Complexity for Active Control of Turbulent Boundary-Layer Noise from Panels," *AIAA Journal*, Vol. 42, No. 7, 2004, pp. 1314–1320.

[10] Herdic, P. C., Houston, M. H., Marcus, M. H., Williams, E. G., and Baz, A. M., "The Vibro-Acoustic Response and Analysis of a Full-Scale Aircraft Fuselage Section for Interior Noise Reduction," *Journal of the Acoustical Society of America*, Vol. 117, No. 6, 2005, pp. 3667–3678.

[11] Lane, S. A., Johnson, M. E., and Fuller, C. R., "Active Control of Payload Fairing Noise," *Journal of Sound and Vibration*, Vol. 290, Nos. 3–5, 2006, pp. 794–819.

[12] Fuller, C. R., "Active Control of Sound Transmission/Radiation from Elastic Plates by Vibration Inputs. 1. Analysis," *Journal of Sound and Vibration*, Vol. 136, No. 1, 1990, pp. 1–15.

[13] Pan, J., Hansen, C. H., and Bies, D. A., "Active Control of Noise Transmission through a Panel into a Cavity: 1. Analytical Study," *Journal of the Acoustical Society of America*, Vol. 87, No. 5, 1990, pp. 2098–2108.

[14] Pan, J., and Hansen, C. H., "Active Control of Noise Transmission Through a Panel into a Cavity: 2. Experimental Study," *Journal of the Acoustical Society of America*, Vol. 90, No. 3, 1991, pp. 1488–1492.

[15] Snyder, S. D., and Hansen, C. H., "Mechanisms of Active Noise Control by Vibration Sources," *Journal of Sound and Vibration*, Vol. 147, No. 3, 1991, pp. 519–525.

[16] Pan, J., Snyder, S. D., Hansen, C. H., and Fuller, C. R., "Active Control of Far-Field Sound Radiated by a Rectangular Panel: A General Analysis," *Journal of the Acoustical Society of America*, Vol. 91, No. 4, 1992, pp. 2056–2066.

[17] Snyder, S. D., and Hansen, C. H., "Design of Systems to Control Actively Periodic Sound Transmission into Enclosed Spaces. Part 1: Analytical Models," *Journal of Sound and Vibration*, Vol. 170, No. 4, 1994, pp. 433–449.

[18] Snyder, S. D., and Hansen, C. H., "Design of Systems to Control Actively Periodic Sound Transmission into Enclosed Spaces. Part 2: Mechanisms and Trends," *Journal of Sound and Vibration*, Vol. 170, No. 4, 1994, pp. 451—472.

[19] Balas, M. J., "Feedback Control of Flexible Systems," *IEEE Transactions on Automatic Control*, Vol. 23, No. 4, 1978, pp. 673–679.

[20] Aubrun, J. N., "Theory of the Control of Structures by Low-Authority Controllers," *Journal of Guidance and Control*, Vol. 3, No. 5, 1980, pp. 444–451.

[21] Meirovitch, L., Baruh,H., and Oz, H., "Comparison of Control Techniques for Large Flexible Systems," *Journal of Guidance, Control, and Dynamics*, Vol. 6, No. 4, 1983, pp. 302–310.

[22] Clark, R. L., "Adaptive Feedforward Modal Space Control," *Journal of the Acoustical Society of America*, Vol. 98, No. 5, 1995, pp. 2639–2650.

[23] Mei, C., Mace, B. R., and Jones, R. W., "Hybrid Wave/Mode Active Vibration Control," *Journal of Sound and Vibration*, Vol. 247, No. 5, 2001, pp. 765–784.

[24] Snyder, S. D., "Active Control: A Bigger Microprocessor Is Not Always Enough," *Noise Control Engineering Journal*, Vol. 49, No. 1, 2001, pp. 21–29.

[25] Elliott, S. J., "Distributed Control of Sound and Vibration," *Noise Control Engineering Journal*, Vol. 53, No. 5, 2005, pp. 165–181.

[26] Borgiotti, G. V., "The Power Radiated by a Vibrating Body in an Acoustic Fluid and Its Determination from Boundary Measurements," *Journal of the Acoustical Society of America*, Vol. 88, No. 4, 1990, pp. 1884–1893.

[27] Baumann, W. T., Saunders, W. R., and Robertshaw, H. H., "Active Suppression of Acoustic Radiation from Impulsively Excited Structures," *Journal of the Acoustical Society of America*, Vol. 90, No. 6, 1991, pp. 3202–3208.

[28] Snyder, S. D., and Tanaka, N., "On Feedforward Active Control of Sound and Vibration Using Vibration Error Signals," *Journal of the Acoustical Society of America*, Vol. 94, No. 4, 1993, pp. 2181–2193.

[29] Elliott, S. J., and Johnson, M. E., "Radiation Modes and the Active Control of Sound Power," *Journal of the Acoustical Society of America*, Vol. 94, No. 4, 1993, pp. 2194–2204.

[30] Currey, M. N., and Cunefare, K. A., "The Radiation Modes of Baffled Finite Plates," *Journal of the Acoustical Society of America*, Vol. 98, No. 3, 1995, pp. 1570–1580.

[31] Johnson, M. E., and Elliott, S. J., "Active Control of Sound Radiation Using Volume Velocity Cancellation," *Journal of the Acoustical Society of America*, Vol. 98, No. 4, 1995, pp. 2174–2186.

[32] Cazzolato, B. S., and Hansen, C. H., "Structural Radiation Mode Sensing for Active Control of Sound Radiation into Enclosed Spaces," *Journal of the Acoustical Society of America*, Vol. 106, No. 6, 1999, pp. 3732–3735.

[33] Gibbs, G. P., Clark, R. L., Cox, D. E., and Vipperman, J. S., "Radiation Modal Expansion: Application to Active Structural Acoustic Control," *Journal of the Acoustical Society of America*, Vol. 107, No. 1, 2000, pp. 332–339.

[34] Griffin, S., Lane, S. A., Hansen, C. H., and Cazzolato, B. S., "Active Structural-Acoustic Control of a Rocket Fairing Using Proof-Mass Actuators," *Journal of Spacecraft and Rockets*, Vol. 38, No. 2, 2001, pp. 219–225.

[35] Cunefare, K. A., Currey, M. N., Johnson, M. E., and Elliott, S. J., "The Radiation Efficiency Grouping of Free-Space Acoustic Radiation Modes," *Journal of the Acoustical Society of America*, Vol. 109, No. 1, 2001, pp. 203–215.

[36] Gardonio, P., Lee, Y. S., and Elliott, S. J., "Analysis and Measurement of a Matched Volume Velocity Sensor and Uniform Force Actuator for Active Structural Acoustic Control," *Journal of the Acoustical Society of America*, Vol. 110, No. 6, 2001, pp. 3025–3031.

[37] Berkhoff, A. P., "Broadband Radiation Modes: Estimation and Active Control," *Journal of the Acoustical Society of America*, Vol. 111, No. 3, 2002, pp. 1295–1305.

[38] Engels, W. P., Baumann, O. N., Elliott, S. J., and Fraanje, R., "Centralized and Decentralized Control of Structural Vibration and Sound Radiation," *Journal of the Acoustical Society of America*, Vol. 119, No. 3, 2006, pp. 1487–1495.

[39] Morgan, D. R., "An Adaptive Modal-Based Active Control System," *Journal of the Acoustical Society of America*, Vol. 89, No. 1, 1990, pp. 248–256.

[40] Lee, C. K., and Moon, F. C., "Modal Sensors/Actuators," *Journal of Applied Mechanics*, Vol. 57, No. 2, 1990, pp. 434–441.

[41] Tanaka, N., Kikushima, Y., and Fergusson, N. J., "One-Dimensional Distributed Modal Sensors and the Active Modal Control for Planar Structures," *Journal of the Acoustical Society of America*, Vol. 104, No. 1, 1998, pp. 217–225.

[42] Sun, D., Tong, L., and Wang, D., "Modal Actuator/Sensor by Modulating Thickness of Piezoelectric Layers for Smart Plates," *AIAA Journal*, Vol. 40, No. 8, 2002, pp. 1676–16797.

[43] Snyder, S. D., Tanaka, N., and Kikushima, Y., "The Use of Optimally Shaped Piezo-Electric Film Sensors in the Active Control of Free Field Structural Radiation, Part 1: Feedforward Control," *Journal of Vibration and Acoustics*, Vol. 117, No. 3, 1995, pp. 311–322.

[44] Hansen, C. H., and Snyder, S. D., *Active Control of Noise and Vibration*, E. & F.N. Spon, London, 1997.

J. Wei
Associate Editor